Mechanics of FRC materials and structures

H. STANG

Technical University of Denmark
Lyngby, Denmark
hs@byg.dtu.dk

1. Integrated structures–materials design

The end goal of design of materials for structural use is always structural performance. Further, all structural designs can be considered to be designed for structural performance, if one defines performance in the broadest sense covering everything from esthetic requirements to durability, load carrying capacity, stiffness, price and more. This text emphasizes the need to use a holistic approach to structural performance involving both materials and structural design. This might seem self-evident, however history has shown that there is a strong need to bring materials and structural design closer together. This is a general statement relevant for all structural materials. Here, however, we restrict ourselves to consider a special class of structural materials, Fiber Reinforced Cementitious Materials or Fiber Reinforced Concrete (FRC).

Conceptually, designing for structural performance involves the optimal selection of material and structural shape. This is the typical regime of structural engineering (except maybe when dealing with esthetic requirements). Traditionally, the menu of construction materials that can be selected for structural applications are rather limited (steel or concrete), so the emphasis is usually placed on designing for the optimum shape given the structural performance requirements. When dealing with mechanical behavior, structural mechanics provides a link between structural shape, materials performance and structural performance, as indicated by the upper triangle in Fig. 1.

Equivalent concepts but on a totally different scale can be found in the regime of the materials engineering, supported by the fundamental discipline of materials science. Materials engineering is illustrated by the lower triangle in Fig. 1. Materials engineering is related to designing materials for
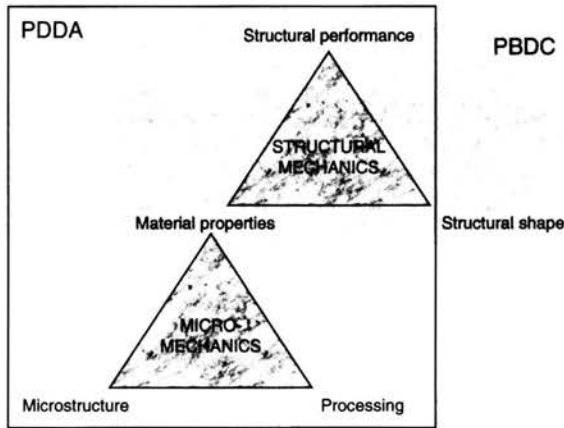
FIGURE 1. Integrated Structures-Materials Design (ISMD) approach illustrated as a merging of two approaches, the Performance Based Design Code approach related to structures, involving structural mechanics and the Performance Driven Design Approach related to materials, involving micromechanics.

performance through manipulation of microstructure and processing. When dealing with mechanical properties of materials the micromechanics provides an important link in this process, as shown in the Figure.

Materials engineering is rarely brought into structural design even though these two fields are related as indicated in Fig. 1. In recent years, however, two separate developments are providing the impetus to alter the traditional approach to structural design. The first development involves fundamental changes in structural design codes, particularly in the US and in Japan. The new Performance Based Design Code (PBDC) shifts from prescriptive requirements in structural detailing (materials and shape) to structural performance specifications. The performance objectives may be specified in terms of operability, repairability, life-safety, or collapse prevention subsequent to specified load levels. This shift in design codes places a greater responsibility on the structural engineer to ensure that the structural design directly links to an expected outcome in performance. However, because of the removal of the detailed, prescriptive nature of the code, structural engineers have greater flexibility in adopting emerging structural materials in the design. The PBDC approach can be thought of as embracing the whole field of structural mechanics, as indicated by the gray rectangle in Fig. 1.

The other recent development which can impact on structural design is the Performance Driven Design Approach (PDDA) of structural materials. In this top-down approach structural performance is the target, from

which the important material property or properties are identified. The relationships between material processing, material microstructure, and material properties are then employed to create materials satisfying the properties required, and thus meeting the targeted structural performance. The conceptual framework of PDDA is shown as the big open square in Fig. 1 embracing the micromechanics triangle as well as part of the structural mechanics rectangle. For PDDA to be successful, the quantitative link between material microstructure, processing and materials properties, provided by micromechanics, is critical.

The conceptual frameworks of the new Performance Based Design Code for structures, and the Performance Driven Design Approach for materials, are complementary to each other, with material property as the common basis and structural performance as the common goal. It is therefore natural to expect synergism when these two frameworks are merged, to form an Integrated Structures-Materials Design approach, or ISMD. A result of this merging is the concept of tailored materials integrated into advanced, optimized structures, for targeted performance, cost-effectiveness and construct-ability. The ISMD approach also provides a rich platform for the collaboration between structural engineers, material engineers, and mechanicians.

Even though Fig. 1 seems to suggest that a single mathematical, mechanics based model can be established to predict structural performance from the material microstructure, material processing and the structural shape, this is not the case at present in any structural field and probably never will be on a routine basis. It is hardly realistic to imagine structural engineers involving microstructural aspects in their structural design except in very special cases. However, it is important to establish an intimate connection between structural and material aspects. In fact the ISMD approach depends on the idea that the world of the structural engineer and that of the material engineer is connected through a common set of concepts, state variables and material parameters. These concepts and parameters become the common denominator of the two worlds.

In the world of micromechanics the primary tasks are to identify the physical mechanisms that govern the material behavior and in this process to establish the relevant length scales for these mechanisms. When this is done the mechanisms are modelled in such a way that an overall material behavior is predicted in an average sense at a larger scale. The overall material behavior is expressed in terms of material parameters. In order to establish an ISMD approach it is essential that these material parameters can be adopted in the models that the structural engineers utilize for prediction of structural performance. In structural models (FEM as well as analytical models) the material parameters are contained in the constitutive relationships which

contain the basic assumptions related to material behavior. It follows that in order to establish an ISMD approach the material engineers involved have to have insight into the methodology used in structural analysis, while the structural engineers have to have insight into the physics and micromechanics of the materials in question.

For routine analysis in engineering applications the structural design tools will be detached from micromechanical modelling. The constitutive models used by the structural designer must be greatly simplified, often resulting in boiling down the material input to a few scalar parameters, while at the same time the models must retain the essential aspects of the physical mechanisms dominating the behavior of the structure. Since the design tools are detached from micromechanical analysis, the structural engineer will not design the construction materials but rather choose material parameters in a realistic range and it is left to the material suppliers to meet the requirements in the most cost effective way.

In practice the establishment of material parameters is done through material testing. In fact, deciding on how to perform material testing becomes a very important part of the establishment of the ISMD approach. In this respect it is important to realize that there are different types of testing which serves different purposes.

The most fundamental type of materials testing – typically carried out in the laboratory – is carried out to derive *basic understanding* of the mechanical behavior of the material in question. The path taken in this type of testing is shown schematically in Fig. 2. Note that in general this cannot be done without some idea of the basic material behavior expressed in terms of a constitutive model. From a materials engineering viewpoint, this constitutive
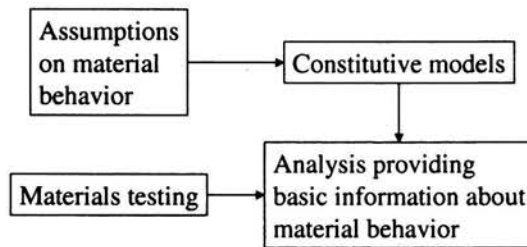

FIGURE 2. Laboratory testing carried out in order to derive basic information about material behavior. After basic assumptions about the material behavior have been formulated in terms of a constitutive model the testing results are analyzed using this model. In this way the analysis provides information about the validity of the constitutive model or provides numerical values for the parameters in the constitutive model.

model should embody linkages between material properties, micro structure and processing, see Fig. 1. After the testing has been carried out the constitutive model is used to interpret the results of the testing. The interpretation of the test requires a structural analysis of the test specimen and loading configuration and will help to shed further light on the assumptions initially made about the material behavior in terms of the validity of the constitutive model or numerical values for the parameters in the constitutive model. Laboratory testing includes both non-standard (research type) testing, and standardized (such as ASTM tests) testing. In standardized testing, much of the specimen size and geometry requirements have been extensively analyzed and codified into simple numerical values.

Another type of testing often used in engineering practice is the testing that is carried out in order to *verify* the material parameters used by the structural engineer in his design. The principle of testing for verification is shown schematically in Fig. 3. This type of testing is also closely connected to a constitutive model, but this time it is the constitutive model applied by the structural designer. Such constitutive models are typically simplified in order to make them operational in a design situation and the number of design material parameters is limited. The structural designer carries out the design based on assumptions regarding the design material parameters, alternatively the design results in requirements on design material parameters. The testing on the other hand provides means to obtaining information about design material parameters through interpretation of the testing results. This interpretation is typically based on a combination of empirical information and detailed analysis of the testing specimen. An example of this type of
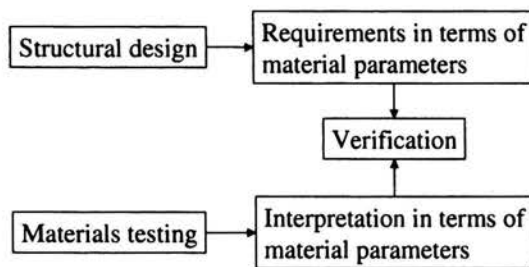
FIGURE 3. The principle of practical testing for verification. Typically, the structural design directly results in requirements for material performance expressed in terms of material parameters. The structural design process applies a simplified constitutive model involving design material parameters. The materials testing involves tools to interpret the test results in terms of these design material parameters. This information is used to confirm the meeting of materials assumptions or requirements in the structural design.

testing is the determination of the cube strength or the cylinder strength of concrete from field cast or cored samples.

Compared to laboratory testing, practical testing must be robust, easy to carry out by field personnel using relatively simple equipment.

The emphasis here is that laboratory testing and practical testing, while having distinctly different purposes, must result in material parameters which are meaningful for both materials engineering and structural design in the context of ISMD (Fig. 1).

Finally, there is the type of testing which is used primarily for comparative purposes. To use this type of testing no assumption about material behavior is required. Typically one or a set of characteristic numbers are derived from the test which can be used for classification of the material in question relative to other materials of the same kind.

To conclude, it should be emphasized that the constitutive models used in practical structural design, while greatly simplified, should be rooted in the more complete constitutive model which form the basis for the laboratory testing. This provides a suitable platform for implementation of the ISMD scheme described previously.

As an example one could take the determination of the behavior of plain concrete in compression. A significant amount of work has been carried out to determine the behavior in uniaxial compression including the ascending and descending part of the stress-strain curve, see e.g. [1, 2]. This kind of testing involves sophisticated test setups and control. The testing can provide information on the microstructural level regarding microcrack formation and localization. Interpretation of the test requires taking the non-linear material behavior into account, as well as the total non-uniform stress-strain field and the relevant boundary conditions – in fact carrying out a structural analysis of the test specimen itself. From this type of testing fundamental knowledge of the influence of microstructure on material performance can be gained.

From a concrete structure design point of view, however, this kind of testing is irrelevant if the design tools do not involve the complete stress-strain curve – which is usually the case. If the design tools and codes only involve the compressive strength obviously only this parameter need to be determined in the test – which can be done in a traditional, standardized test with associated formulae connecting the measured maximum load with the design uniaxial compressive strength. Ideally, this connection between measured properties and simplified material parameters should be established through a careful theoretical and experimental analysis of the test arrangement, often, however, this is established by empirical means.

In practice the second type of testing is very important and it is crucial that it is robust and easy-to-use. Often it is difficult to establish simple

testing methods which give direct information about a given material parameter. However, the testing methodology should reflect as closely as possible the material parameters used in design, thus ruling out many of the testing methods appropriate only for relative ranking of material performance.

A suitable testing methodology makes it possible to establish material specifications in terms of the testing results. Also material suppliers can utilize the testing strategy and material specifications for providing appropriate data for their specific materials as well as for further optimization and development based on micromechanical models.

2. FRC in light of ISMD

Fiber Reinforced Concrete (FRC) has been in existence for a long time. Historically, Egyptians around 1500 BC employed straws to reinforce mud bricks which otherwise would become very brittle upon drying. In some parts of China and Japan, clay walls build around 5000 BC were reinforced by thin strips of bamboos. Thin sheet cement products reinforced with asbestos fibers have been in production by the Hatcheck process since the early 1900s. Concrete reinforced with steel wires and fibers can be traced back to the patents of Joseph Lambot in 1847 and A. Berard in 1874 (see the historical overview by Naaman [3]) and more recently, the work of Romualdi and Batson [4] and Romualdi and Mandel [5]. Since then, an increasing variety of fibers, including steel, polymeric (polypropylene, polyethylene, polyvinyl alcohol, aramid, acrylic, nylon, etc.) and natural (asbestos, cellulose, sisal, etc.), as well as glass and carbon fibers have been applied to concrete, mortar or cement reinforcement in continuous and discontinuous forms, employing a variety of processes (e.g. the Hatchek process, SIFCON, shotcreting, extrusion and regular casting).

Most of these FRCs are used in non-structural applications or in secondary elements, meaning that the fibers are employed to serve functions such as minimizing shrinkage cracking and limit crack widths due to mechanical loading. Structural use of FRC is scarce, and attempts to use fiber reinforcement as structural reinforcement has so far been concentrated on replacement of shear reinforcing stirrups in structural members such as beams as well as replacement of complicated reinforcement arrangements in areas where concentrated loading is applied to the structure.

Thus, while extensive amounts of research have been carried out in FRC, the expected pervasive use of FRC in the construction industry has not materialized. There are a number of possible reasons for this phenomenon. Conceptually, while FRC is generally recognized as tougher than concrete, a logical and systematic translation of this property into structural performance is all

but absent. On a practical level, current design codes for structures do not usually cover FRC materials. Without design guidelines, engineers find it difficult to incorporate this material into their structural design. Secondly, test methods that are robust and at the same time properly characterize FRC are still under debate. Thirdly, without a rational methodology for selection of fiber, matrix and control of interface, the resulting composite usually does not achieve optimal behavior, thus negatively affecting the performance to cost ratio.

While the conceptual and practical frameworks for structural design described earlier are general for all materials, they are particularly relevant for fiber reinforced concrete (FRC) in light of the obstacles faced by potential users of FRC. However, as it will be demonstrated in the present text, many of the elements necessary for establishing an ISMD approach to FRC are in place or presently emerging.

In recent years, significant amount of research has been conducted in the micromechanics of fiber reinforced concrete, relating fiber, matrix and interface properties to composite mechanical properties. The increasing range of fibers available, the deepening knowledge of interface properties control, and the substantial information on the mix design of concrete materials, lead to fiber reinforced concretes with wide ranging properties. FRC can now be tailored to behave in a quasi-brittle manner or exhibit strain-hardening in tension.

The possibility of meeting targeted structural performance, with judicious use of tailored FRC is increasingly realistic. Significant enhancements in structural ductility, damage tolerance, energy absorption, fatigue resistance, and other desirable behaviors that support various levels of structural performance objectives can be expected. A Performance Based Design Approach for FRC was first proposed by Li [6], providing a rational basis for fiber selection, matrix design and interface tailoring.

Also on the structural level significant progress is being made. The compressive strength is a well known material property which is embodied into design codes, and used extensively by structural engineers. It is also a property which can be tested relatively simply. Similar simple, scalar types of material properties characterizing toughness which can be incorporated in structural design models, are being proposed for tension-softening FRC [7, 8, 9].

These relatively simple methods of characterizing tension-softening FRC provides multiple advantages. On the one hand, they capture the essence of the effect of fibers as load carrying elements in the FRC composite, and the parameters can be incorporated into design approaches relatively easily. On the other hand, the parameters can be determined or verified in a routine manner using a robust testing methodology such as the flexural test with a

notched beam. Thus, these toughness parameters for softening FRC can be considered the equivalent of compressive strength for normal concrete. The methodology also makes it easier for material suppliers, such as fiber producers, and ready mix suppliers, to meet material specifications in a construction project in the most cost effective way.

For strain-hardening FRC, the uniaxial tensile stress-strain curve together with crack width development during strain hardening provide the most important material properties for structural design approach. The uniaxial tension test is easy to conduct, as there is no instability associated with softening in this material.

A few design guidelines for strain hardening materials do exist aiming specifically at sprayed glass fiber reinforced concrete (GFRC) which can be considered a strain hardening material [10, 11]. The basis of these guidelines is a representative stress-strain relationship, however the design methods proposed are purely based on linear elasticity.

3. Constitutive modeling

3.1. Toughness, ductility and constitutive models

On a macroscopic level basically two types of mechanical behavior is observed for FRC-materials. The materials are typically characterized and most easily identified in uniaxial tension. In the uniaxial tension stress field the first type of behavior is dominated by the formation of a single crack. The propagation of this single crack is greatly influenced by the fibers as will be discussed in a later section, however the bulk behavior of the fiber reinforced material is not fundamentally different from the bulk behavior of the matrix, neither strength nor stiffness is significantly influenced by the fibers. A material with this type of behavior is in the present text called *Tension Softening FRC* or simply *FRC material*.

The second type of material is characterized by the fact that many, parallel cracks are formed after the formation of the first, when the material is subjected to uniaxial tension. Each of these cracks have a limited crack opening (typically less than 100-200 μm), in fact additional straining of the material is associated with the formation of multiple cracks rather than opening of the one single crack. Some additional crack opening of all cracks is occurring simultaneously, and at some point one single crack starts to open and material failure then takes place through opening of this particular crack. A material with this type of behavior is called a *Strain Hardening FRC* or simply *SHFRC* due to the fact that the stress level for additional crack formation is increasing with increasing number of cracks and increasing average strain.

It immediately follows from the above, that in the case of FRC materials the influence of fibers is in enhancing the resistance to crack propagation resulting in an increase in composite *toughness*. Correspondingly a fracture mechanical approach should be adopted in order to describe the influence of fibers on crack propagation while the bulk concrete material can be treated in a standard fashion. In the fracture mechanical approach the influence of fibers on composite properties should be represented in an average way in terms of fracture mechanical parameters. These fracture mechanical parameters should be determined averaging over an area on the crack surface large enough to contain a reasonable amount of fiber this area can be described as a representative area. How large such an area should be depends on the fiber size and fiber amount.

In the case of a SHFRC material the influence of fibers is in enhancing the tensile strain-capacity leading to an increase in material *ductility*. Correspondingly, the constitutive model should be a continuum model and the representative volume element used for determination of the stress-strain relationship should contain a sufficient number of cracks so that the concept of average stress and strain makes sense. The representative volume element should be much larger than the crack spacing when the material has reached the so-called crack saturation point. Note, that since formation of cracks is a discrete process there is a problem in defining a representative volume element when only a few cracks have been formed. This problem is overcome, however, by assuming that the presence of a few cracks with limited crack opening does not influence the overall structural behavior.

In both the above cases the material microstructure defines a characteristic scale. In the case of FRC a representative area is defined with a certain minimum size related to fiber size and fiber content. In the case of SHFRC a representative volume element is defined with a certain size which is related to crack spacing (which is also related to the fiber, interface and matrix properties – as it will be shown later). Since, after the averaging has been completed, the representative area and volume element represent a material point in constitutive modelling, these areas and volumes have to be small in some sense relative to the structure that the constitutive model is used to describe. Otherwise the assumptions used in the averaging process become invalid.

In Fig. 4 the constitutive modelling is shown in a schematic way indicating the structural scale together with the representative crack area and the representative volume element of the FRC and SHFRC material, respectively.

In the following special emphasis will be placed on the FRC materials and the special problems related to material characterization, testing and structural analysis.
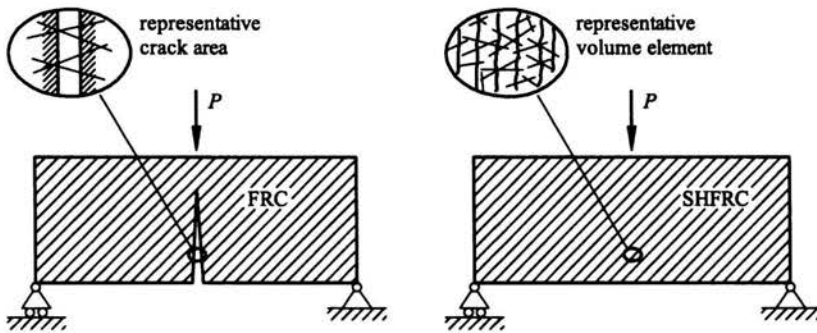
FIGURE 4. The modelling of FRC and SHFRC structures according to the present concept: the FRC material (left) is modelled as a homogeneous material using a fracture mechanical approach. On the the crack surface the presence of the fibers is taken into account in an average sense. The SHFRC material (right) is modelled also as a homogeneous material but using a continuum approach with a constitutive relation derived from a representative volume element containing multiple cracks.

3.2. Fracture models

Fracture mechanics of concrete is a relatively young field compared to e.g. fracture mechanics of metals. The first significant attempts to develop a non-linear fracture mechanics framework for concrete were taken in the sixties after it had been realized that linear fracture mechanics could not be applied. In Karihaloo [12] a comprehensive overview of experimental documentation for the inability of linear elastic fracture mechanics to describe fracture phenomena in concrete can be found.

Conceptually, crack propagation in concrete is described referring to a zone of diffuse microcracking – the process zone, and a localized crack. The localized crack can be divided into a part where aggregate interlock is present and a "true" traction free crack.

A remarkable simple description of crack formation in plain concrete was suggested by Hillerborg et al. [13].

Hillerborg suggested the so-called Fictitious Crack Model, (FCM) which originally was intended for use in combination with FEM, however as it will be shown throughout this lecture the approach can easily be adopted in analytical models also.

The fictitious crack model is often referred to as cohesive crack model. However, the term *cohesive crack* also has a much broader meaning (e.g. cohesive interface crack models are defined below), thus there is good reason to refer to the original name *FCM*.

The fictitious crack model – originally defined only in mode I, relies on a number of simple assumptions:

- Everything (process zone, localized crack with aggregate interlock and localized traction free crack) can be modelled with a single crack plane.

- The energy dissipation at the fictitious crack tip is negligible compared to the energy dissipation in the process zone and along the localized crack where aggregate interlock is present and interface frictional slippage is taking place.

- The process zone, as well as part of the localized crack where aggregate interlock is present can be modelled by a fictitious crack which is characterized by the stress-crack opening relationship, where the stress carried across the crack σ_w depends on crack opening w.

- The length of the fictitious crack cannot be assumed to be small compared with a typical structural dimension.

In Fig. 5 a real crack is outlined together with the fictitious crack model of the same crack.
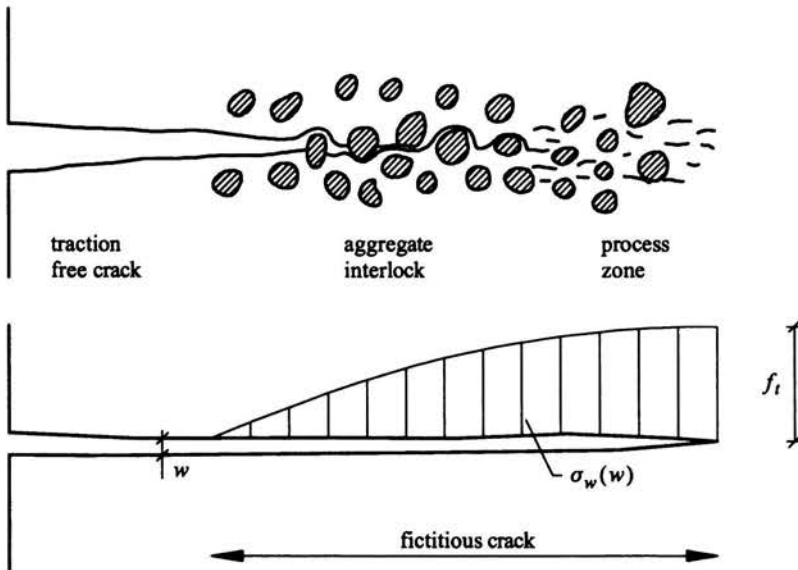

FIGURE 5. Outline of a concrete crack and the essential features: the process zone, aggregate interlock and traction free crack together with the fictitious crack model.

From a modelling point of view the first assumption makes application of the FCM in FEM formulations particularly simple.

The second assumption means that stress-singularities can be disregarded. As soon as the largest principle tensile stress reaches the tensile strength a fictitious crack is formed or, if a crack is already present, extends.

The third assumption means that the basic fracture parameter is the stress-crack opening relation $\sigma_w(w)$. It is usually assumed that this function is a monotonically decreasing function, indicating softening behavior. It is furthermore assumed that:

$$\sigma_w(w = 0) = f_t \tag{3.1}$$

where f_t is the tensile strength. A characteristic crack opening w_c is defined by:

$$\sigma_w(w_c) = 0. \tag{3.2}$$

The stress-crack opening relation can be characterized in terms of the area under the curve and since no energy dissipation is assumed to take place at the crack tip, this area can be associated with the fracture energy:

$$G_F = \int\limits_0^{w_c} \sigma_w(w)\, dw. \tag{3.3}$$

From a modelling point of view, any constitutive continuum modelling can be chosen in the bulk material. Often a simple linear elastic modelling is chosen. Introducing the Young's modulus E the characteristic length l_{ch} can be defined:

$$l_{ch} = \frac{EG_F}{f_t^2}. \tag{3.4}$$

The characteristic length can be used to characterize the brittleness of a given material but can also be used to define a dimensionless structural brittleness number B by taking the ratio of a characteristic structural length L to the characteristic length of the material:

$$B = \frac{Lf_t^2}{EG_F} \tag{3.5}$$

introduced by Hillerborg et al. [13].

A simple illustration of the significance of the brittleness number can be made by considering the simple example of a concrete bar of length L, restrained from longitudinal movement at both ends, undergoing shrinkage ε_s, where ε_s is positive when the material contracts.

Assume that the material outside the crack is linear elastic with tensile strength f_t and elastic modulus E. In the bulk material the stress state is

assumed to be uniaxial, thus the following constitutive relationship governs the bulk material behavior:

$$\sigma = E(\varepsilon + \varepsilon_s) \tag{3.6}$$

where ε is total strain.

Assume further that the stress-crack opening relationship is linear, i.e. given by:

$$\sigma_w(w) = \begin{cases} f_t(1 - \dfrac{w f_t}{2G_F}) & \text{for } w \leq \dfrac{2G_F}{f_t}, \\ 0 & \text{for } w > \dfrac{2G_F}{f_t}, \end{cases} \tag{3.7}$$

and that crack growth is initiated when the largest principle tensile stress in the concrete reaches f_t. The situation is illustrated in Fig. 6.
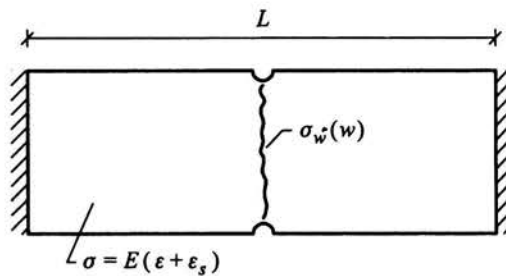

FIGURE 6. Schematic representation of the restrained concrete bar and the constitutive modeling associated with the analysis.

For any shrinkage stress $\varepsilon_s < f_t/E$ the concrete bar remains un-cracked. Assuming that a weak cross section is present in the concrete bar – in Fig. 6, a weak cross section is symbolized by a cross section with a slightly reduced cross sectional area – a stress softening is introduced as $\varepsilon_s \to f_t/E$. Assuming further, that the softening takes place uniformly over the weak cross section. A simple solution for the crack opening as function of the shrinkage can be derived realizing that the uniaxial stress σ is the same in the bulk material and at the crack:

$$\sigma = \sigma_w(w) \tag{3.8}$$

and that the total elastic deformation $L\varepsilon$ and the crack opening w together must satisfy the restraining condition:

$$L\varepsilon + w = 0. \tag{3.9}$$

The solution reads:

$$
w = \begin{cases}
\dfrac{L(\varepsilon_s - \varepsilon_t)}{\left(1 - \dfrac{L f_t^2}{2EG_F}\right)} & \text{for } \varepsilon_t \leq \varepsilon_s \leq \dfrac{2G_F}{f_t L}, \\[3ex]
L\varepsilon_s & \text{for } \dfrac{2G_F}{f_t L} < \varepsilon_s,
\end{cases}
\tag{3.10}
$$

where

$$
\varepsilon_t = \frac{f_t}{E}.
\tag{3.11}
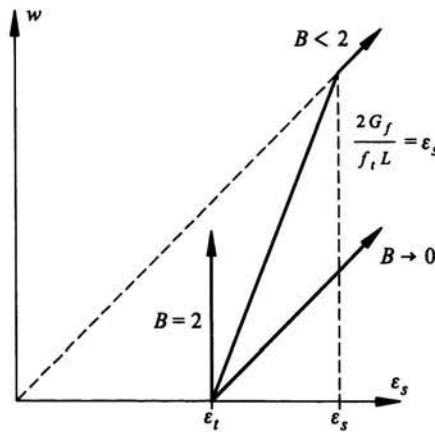$$

The solution is illustrated in Fig. 7.

FIGURE 7. The solution for the problem of the restrained concrete bar undergoing shrinkage. The crack opening w is plotted as function of imposed shrinkage for varying brittleness number B. Unstable crack opening is obtained for $B \geq 2$.

The fracture mechanical approach easily captures a number of significant material and structural related aspects.

It follows from Eq. (3.10) that the structural behavior immediately after the crack has been formed is dictated by the brittleness number B defined above. For $B \geq 2$ the crack opens in an unstable way: an infinitesimal increase in shrinkage over ε_t results in a finite increase in crack opening. The most stable situation is obtained when $B \to 0$ where the crack opens in the same way that the concrete bar contracts, if it is not restrained:

$$
\frac{dw}{d\varepsilon_s} \to L \quad \text{for} \quad B \to 0.
\tag{3.12}
$$

A number of important consequences follow from this solution which has significant implications for development of FRC-materials: increasing only

the fracture energy and leaving the rest of the material parameters unchanged reduces crack opening for certain levels of imposed strain and can change unstable crack formation to stable crack formation. The larger the size of the structure (L) and the higher the strength of the material (f_t), the larger fracture energy is required to obtain stable crack opening. No matter how high the fracture energy a certain size dependency is maintained in the way that a crack opens (Eq. (3.12)). These aspects have always been governing the development of FRC materials in a qualitative way, however, a fracture mechanics approach is obviously able the quantify the approach.

Though similar in many aspects, in one aspect the FCM approach for crack propagation and opening in FRC differs significantly from the FCM approach to concrete fracture. Since the stress transfer across the crack surfaces is closely related to the fibers debonding and pulling out and since the fibers often have a length which is not small compared to crack openings accepted in real structures, from a practical point of view, the parameter w_c is not relevant. This implies that in analysis of FRC materials, G_F defined by Eq. (3.3) looses its significance from a practical, structural point of view. Furthermore, as it will be shown in the following, the stress-crack opening curve can take quite different shapes. Thus, the actual variation of the function $\sigma_w(w)$ in the range of acceptable crack openings – say 0-0.5 mm – becomes more important than G_F.

3.3. Fracture mechanics for FRC

The stress-crack opening relationship lends itself in a very natural way to the description of fracture of short fibre reinforced materials with FRC behaviour. In fact the fictitious crack approach was suggested by Hillerborg et al. [14] for use in the description of formation of cracks in fibre reinforced concrete introducing, an approach where the stress-crack opening relationship now describes the stresses carried by fibres across a tensile crack in the composite material as function of the crack opening. Later this approach has been taken by numerous authors in attempts to describe the crack bridging ability of fibres – the so-called fibre bridging – in different brittle matrix composite systems, [6, 15, 16, 17, 18]. The fictitious crack in FRC materials now represents the process zone, aggregate interlock as well as fibre bridging, see Fig. 8.

Conceptually the fiber bridging is understood as the average effect of fibers being *debonded* and *pulled out*. This debonding and pulling out can be modelled on a micro-mechanical basis assigning fracture mechanical properties to the interface. The pulling out of a single fiber can be considered an elementary case from which the average response can be obtained through
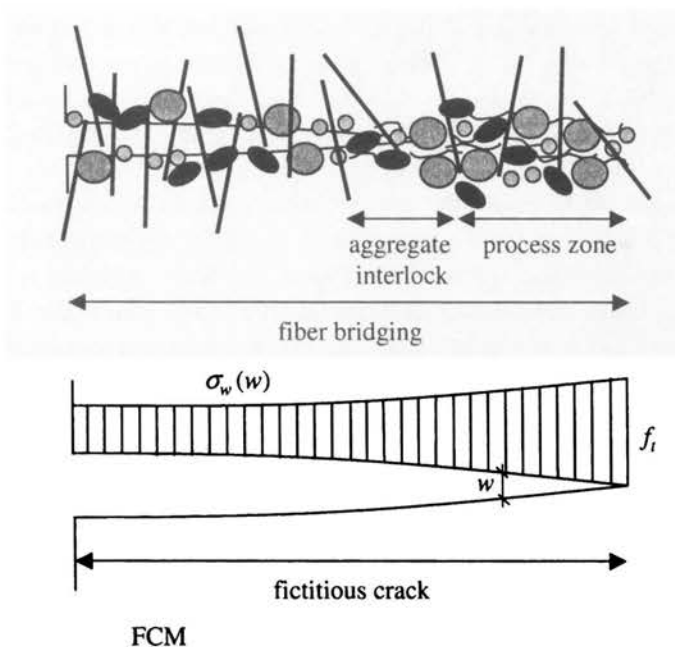
FIGURE 8. A crack in SFRC and the essential features: zone with fibre bridging, the process zone and aggregate interlock together with the FCM.
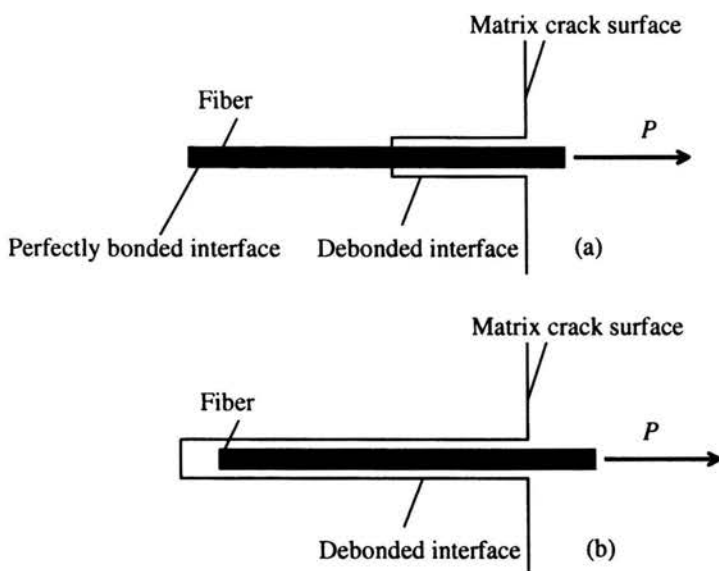

FIGURE 9. The concept of a single fiber bridging a matrix crack and being debonded and pulled out as the crack opens up.

an averaging process taking different fiber embedment lengths and fiber orientations into account [6]. The concept of fiber debonding and pulling out is shown in Fig. 9. The average fiber bridging contribution can be added to the concrete contribution to form the stress-crack opening relationship for the composite materials, see Fig. 10, Li et al. [15].

Though similar in many aspects, in others the FCM approach for crack initiation, propagation and opening in FRC differs significantly from the FCM approach to concrete fracture. Since the fibre bridging is closely related to the fibres debonding and pulling out, and since the fibres often have a length that is not small compared to crack openings accepted in real structures, from a practical point of view, the parameter w_c is not relevant. This implies that in analysis of FRC materials, G_F defined by Eq. (3.3) loses its significance from a practical, structural point of view. Furthermore, the stress-crack opening curve shape depends on the type and amount of fibre used, and the shape of the curve influences the structural behaviour. Thus, the actual variation of the function $\sigma_w(w)$ in the range of acceptable crack openings – e.g. 0-1.5 mm – becomes more important than G_F.

Finally, it is very important to realize that in many practical applications the fibres are not randomly distributed. As a consequence, the stress-crack opening relationship of FRC materials cannot be considered an isotropic property, i.e. the relationship depends on the direction of cracking relative to the fibre orientation. Often the fibres are oriented during the casting process. In surface layers fibres are to a certain extent oriented parallel to the external surface (the so-called wall effect) and sometimes the thickness of the structural member is of the same order of magnitude as the fibre length (e.g. pavements), which causes fibres to be oriented throughout the thickness of the structural member.

4. Stress-crack opening relationships for design

4.1. General

Experimental determination of the stress-crack opening relationship can be done in a fundamental way using the uniaxial tension test [19, 20, 21]. As mentioned in the previous section, the shape of the stress-crack opening relationship depends heavily upon the type and amount of fibre used. The relationship can be divided into a concrete contribution and a fibre contribution. The concrete contribution is the softening stress-crack opening relationship for the un-reinforced concrete, while the fibre contribution consists of a steeply ascending part followed by a slowly descending or softening part. The first part of the resulting relationship – up to crack openings of about
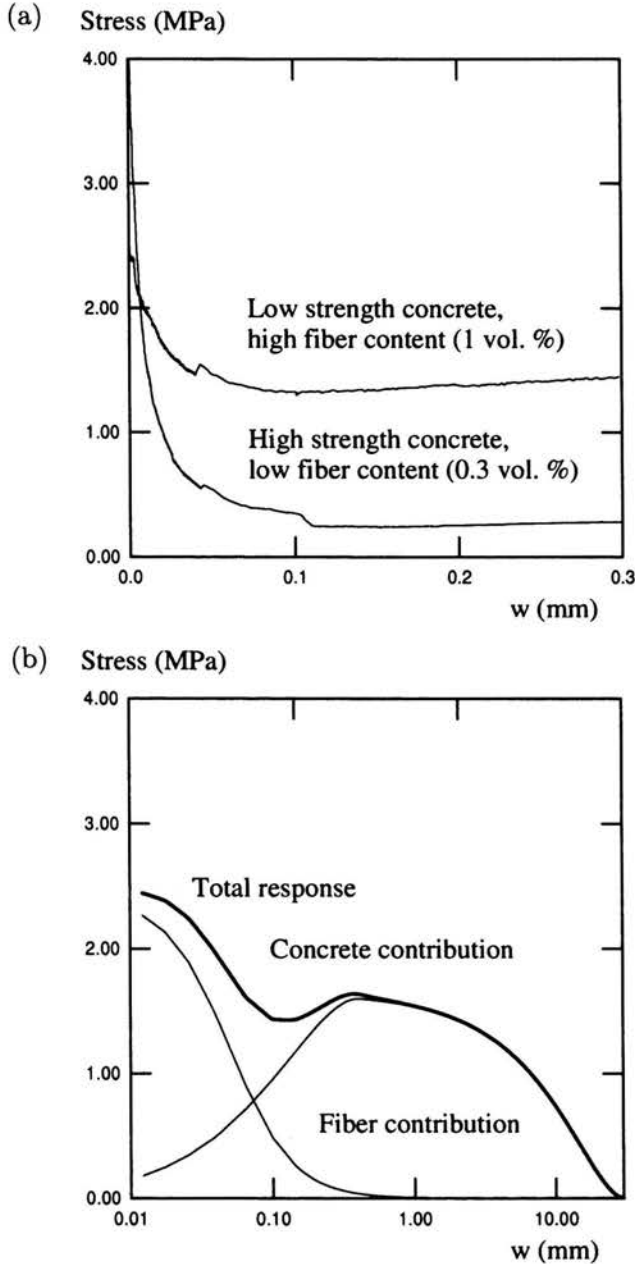
(a)   Stress (MPa)

(b)   Stress (MPa)

FIGURE 10. Typical stress-crack opening relationships (a) obtained from experimental measurements on steel fibre reinforced concrete containing 0.3 and 1 vol.% of hooked end steel fibres in high and low strength concrete, respectively. In (b) is shown a conceptual theoretical modelling of the relationship, following Li et al. [15], showing the concrete and the fibre contributions. (Note the logarithmic length scale).

0.1-0.2 mm – is a result of the competing concrete and fibre contribution, while the relationship for larger crack openings is due mainly to the fibre contribution. The resulting total response consists of first a descending part, then a slowly ascending and finally a descending or softening part, see Fig. 10.

For design purposes, simplified versions of the stress-crack opening relations need to be defined.

4.2. Multi-linear relationship

Very realistic representations of measured stress-crack opening relationships can be obtained with a multi-linear function:

$$\sigma_w = \sigma_i - \alpha_i w, \qquad w_{i-1} < w \le w_i = \frac{\sigma_{i+1} - \sigma_i}{\alpha_{i+1} - \alpha_i},$$

$$w_0 = 0, \qquad \sigma_1 = f_t, \qquad \alpha_1 > 0. \tag{4.1}$$

The multi-linear stress-crack opening relationship is illustrated in Fig. 11. As indicated in Fig. 11 the slopes α_i of the different linear sections of the multi-linear function can be positive and negative. It is assumed, however, that the tensile strength is never reached again after softening has been initiated.
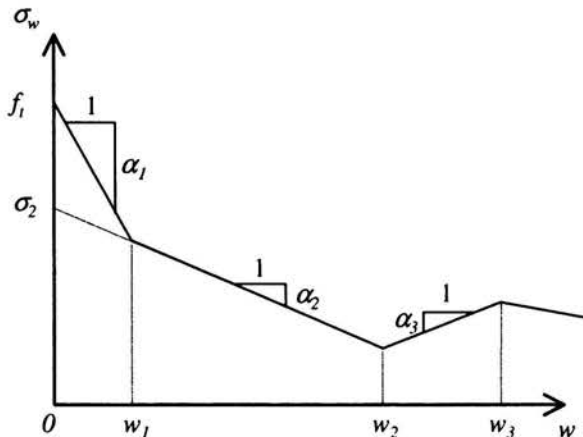

FIGURE 11. Illustration of the multi-linear stress-crack opening relationship. Here: α_1 and α_2 are positive, α_3 is negative.

4.3. Bi-linear relationship

For many FRC materials a bi-linear relationship provides a reasonable representation of the measured behaviour, compare with Fig. 10:

$$\sigma_w(w) = \begin{cases} \sigma_1 - \alpha_1 w & \text{for } 0 \leq w \leq w_1 = \dfrac{\sigma_2 - \sigma_1}{\alpha_2 - \alpha_1}, \\[2mm] & \alpha_1 > 0, \quad \sigma_1 = f_t, \\[2mm] \sigma_2 - \alpha_2 w & \text{for } w_1 < w \leq w_c = \dfrac{\sigma_2}{\alpha_2}, \quad \alpha_2 > 0. \end{cases} \tag{4.2}$$

In this approach a total of four material parameters are required to describe the stress-crack opening relationship.

The bi-linear stress-crack opening relationship is illustrated in Fig. 12. In the limiting case where α_1 becomes very large compared to α_2, the bilinear relationship becomes what is called a drop-linear relationship, reducing the number of parameters to three.
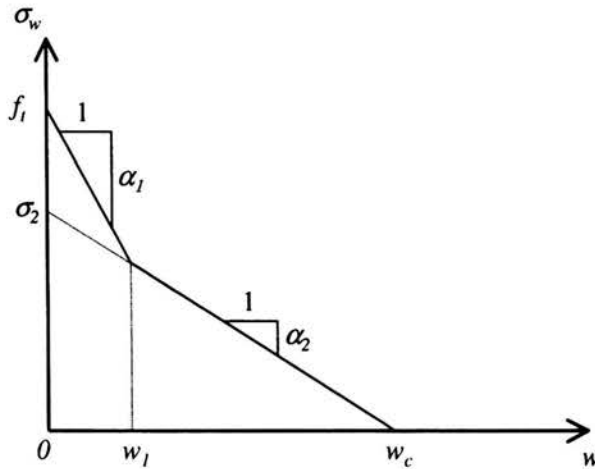

FIGURE 12. Illustration of the bi-linear stress-crack opening relationship.

4.4. Drop-constant relationship

An even more simple representation which has obvious advantages from a design point of view is the so-called drop-constant relationship:

$$\sigma_w(w) = \begin{cases} f_t & \text{for } w = 0, \\[2mm] \sigma_y & \text{for } w < w_{max}, \end{cases} \tag{4.3}$$

defining a *residual strength* σ_y which characterizes the relationship up to a certain maximum crack opening w_{max}.

In this approach a total of two (or three – counting w_{max}) material parameters are required to describe the stress-crack opening relationship.

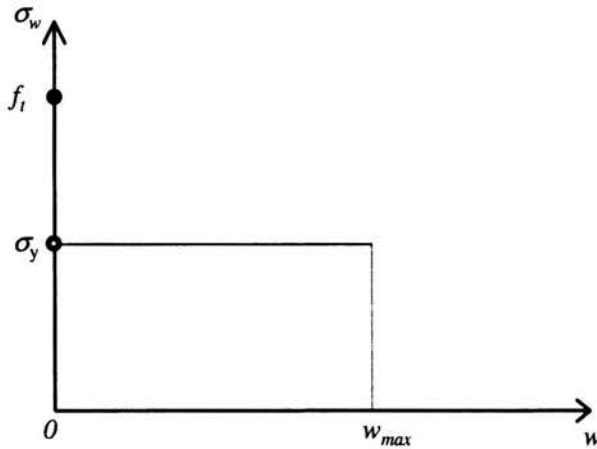The drop-constant stress-crack opening relationship is illustrated in Fig. 13.

FIGURE 13. Illustration of the drop-constant stress-crack opening relationship.
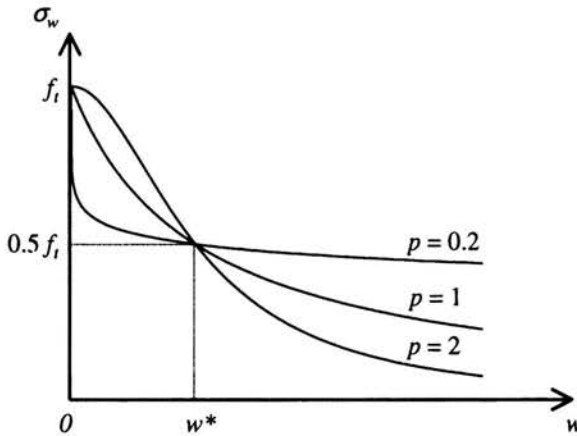

FIGURE 14. Illustration of the free-form stress-crack opening relationship and the influence of the shape parameter p for a fixed value of w^*.

4.5. Free-form relationship

Stang and Aarre [22] showed that the σ–w relationship of the form (4.4) can be used to model a large variety of FRC materials using empirical variations of the parameters w^* (reference crack width) and p (shape parameter):

$$\sigma_w(w) = \frac{f_t}{1 + \left(\dfrac{w}{w^*}\right)^p}. \tag{4.4}$$

Again, two material parameters are associated with the model. The free-form stress-crack opening relationship is illustrated in Fig. 14.

4.6. Characteristic values and safety factors

The analysis of FRC structures based on the material parameters described above should be carried out according to the principles known from standard concrete structural analysis and design.

Thus, based on materials testing, an average and a characteristic response should be identified, see below. Analysis in the serviceability limit state should be based on assumed or measured characteristic values, while analysis and design in the ultimate limit state should be based on characteristic values modified with safety factors. At this stage only limited experience has been gained with structural design based on fracture mechanical principles. Safety factors should be code related. It is outside the scope of the present document to give specific values.

In design of minimum reinforcement and design for crack widths in traditional reinforced concrete structures, the under-estimation of tensile strength, f_t can lead to non-conservative results regarding safety and crack openings. Similarly in FRC structures, both the upper and lower characteristic value of f_t should be considered depending on which results in the more critical situation. The lower characteristic value of $\sigma_w(w)$ for $w > 0$ will always result in the more critical situation.

4.7. Experimental determination and verification

For experimental determination of the stress-crack opening relationship it is useful to distinguish between tests aiming for direct determination of the relationship and methods aiming for verification of a simplified version of the relationship used in design. In this context it should be noted that no generally accepted standards for either direct determination or verification of the stress-crack opening relationship exist at this point in time.

Methods for direct determination of the stress-crack opening relationship are typically based on a uniaxial tension testing configuration.

A standard for uniaxial tension testing method for FRC (as well as other types of FRCC) has been proposed in [21]. Here a method for the direct determination of the characteristic stress-crack opening curve $\sigma_{w,k}(w)$ from the average curve $\overline{\sigma}_w(w)$ is described. Care must be taken to obtain a fibre orientation in the test specimen that is representative of the orientation in the structural application, see Sec. 3.3. The uniaxial tension test method is not suitable for determination of the tensile strength f_t. It is assumed that information about the characteristic and design tensile strengths, $f_{t,k}$ and $f_{t,d}$ is obtained independently, through codes or standard testing methods intended for plain concrete. The principle is illustrated in Fig. 15.
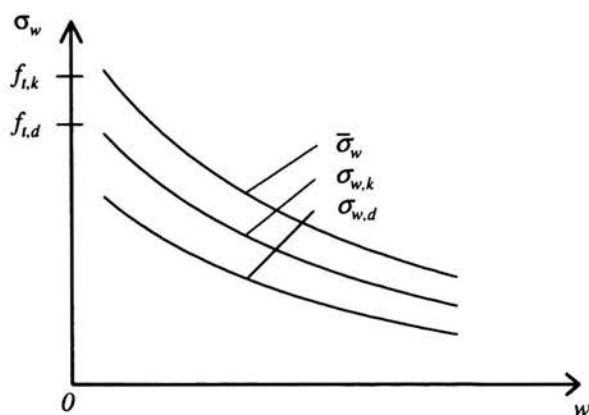

FIGURE 15. Illustration of average, $\overline{\sigma}_w(w)$, characteristic, $\sigma_{w,k}(w)$, and design, $\sigma_{w,d}(w)$, stress-crack opening relationships. The average and the characteristic curves are based on testing experience. The design curve is related to the characteristic curve through a safety factor. The characteristic tensile strength $f_{t,k}$ and the design value $f_{t,d}$ are code related properties or properties obtained from independent testing.

A stress-crack opening curve for use in serviceability limit state analysis may be obtained from the uniaxial testing result and information about tensile strength using curve fitting of any of the suggested material models, Eqs. (4.1) to (4.4) to the characteristic stress-crack opening relationship. It is recommended that the fitted analytical relationship always lies below the characteristic curve. Furthermore, the fitted stress-crack opening relationship should always be overall descending, i.e. the characteristic tensile strength should never be reached again.

The design stress-crack opening relationship $\sigma_{w,d}(w)$ for use in ultimate limit state analysis is obtained from the characteristic relationship based on the lower characteristic tensile strength by division with a safety factor.

Experimental verification of assumed stress-crack opening curves can be carried out through a direct comparison with uniaxial test data. Stang and Olesen [23] suggested to carry out bending tests with a notched beam, e.g. according to [24], and to compare the test results with pre-calculated, expected responses. The expected response can be calculated for any of the suggested material models, Eqs. (4.1) to (4.4). This method is still under investigation.

It should also be noted that much work has been carried out in order to set up methods of inverse analysis to derive the stress-crack opening relationship from bending tests [25, 26]. Some difficulties with this type of approach were pointed out in Stang and Olesen [27].

5. Cross sectional analysis for flexure and axial forces

5.1. General – non-linear hinge

A cross-sectional analysis of the cracked section of e.g. a beam, a pipe or a slab can be carried out by describing the cracked section as a non-linear hinge.

The idea of the non-linear hinge model is to analyze separately the section of the structural element where the crack is formed and assume that the rest of the structure behaves in a linear elastic fashion. In order for the non-linear hinge to connect to the rest of the structure, the end faces of the non-linear hinge are assumed to remain plane and to be loaded with the generalized stresses in the element.

The principle of the analysis in the case of a structural element subjected to a combination of flexure and axial force is shown in Fig. 16. The structural
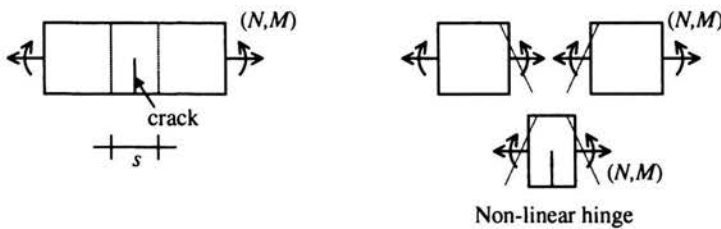
FIGURE 16. The principle of the non-linear hinge analysis in the case of a structural element subjected to a combination of flexure and axial force (left). As shown in the right hand side, the element is divided into a middle section of width *s* containing the crack – the so-called non-linear hinge – and the rest of the element which is assumed to behave elastically. The non-linear analysis for crack propagation and associated load carrying capacity is carried out only for the non-linear hinge.

element is divided into a non-linear hinge of length s where the main non-linear behaviour due to cracking is concentrated and into other parts that are considered to behave elastically.

The non-linear analysis for fictitious crack propagation and associated load carrying capacity is carried out only for the non-linear hinge loaded with the generalized stresses, in this case an axial force N and a moment M.

5.2. Geometrical assumptions

A number of different solutions for rectangular cross section can be found in the literature based on different assumptions regarding kinematic and constitutive conditions. An overview of different constitutive relations in terms of the stress-crack opening relation governing the traction on the fictitious crack as function of the crack opening can be found above.

Different kinematic assumptions applied in various models are shown schematically in Fig. 17 and can be described in the following way:

- The fictitious crack surfaces remain plane and the crack opening angle equates the overall angular deformation of the non-linear hinge (Pedersen [28]), see Fig. 17(a).

- The fictitious crack surfaces remain plane and the crack opening angle equates the overall angular deformation of the non-linear hinge. Furthermore, the overall curvature of the non-linear hinge, the curvature of
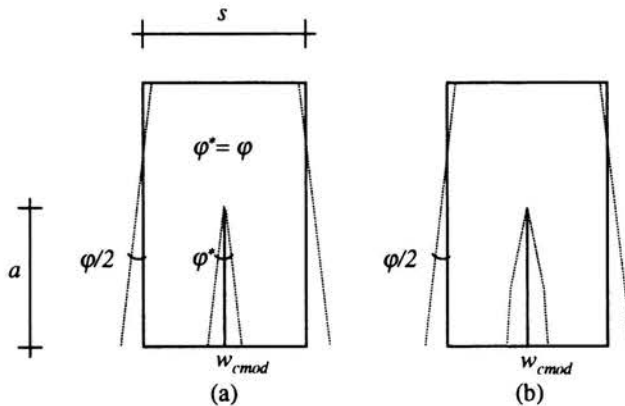

FIGURE 17. Different kinematic assumptions applied in various non-linear hinge models. In (a) the fictitious crack surfaces remain plane and the crack opening angle equates the overall angular deformation. In (b) the fictitious crack surfaces do not remain plane, the deformation is governed by the stress-crack opening relationship.

the cracked part and the curvature of the elastic part are linked based on an assumption of parabolic variation of the curvature [29, 30], see Fig. 17(a).

- The fictitious crack surfaces do not remain plane, the deformation is governed by the stress-crack opening relationship, the crack length and the overall angular deformation of the non-linear hinge, see Ulfjkaer et al. [31] for linear stress-crack opening relationship, and Olsen [32] for a bi-linear stress-crack opening relationship and the drop-linear relationship, see Fig. 17(b).

In all cases the average curvature of the non-linear hinge, κ_m is given by:

$$\kappa_m = \frac{\varphi}{s}. \tag{5.1}$$

In the first two approaches, the crack mouth opening displacement w_{cmod} (the crack opening at the bottom of the non-linear hinge) follows directly from the crack opening angle φ^* and the length of the fictitious crack, a:

$$w_{cmod} = \varphi^* a, \tag{5.2}$$

while the crack mouth opening displacement in the third approach is determined from the stress-crack opening relationship, the overall curvature κ_m and the length of the fictitious crack.

5.3. Analysis for rectangular sections

The analysis according to the three different kinematic assumptions is presented below. In all cases the solutions can be generalized to cover T-sections, non-linear material behaviour in compression etc.

5.3.1. Simplified approach by Pedersen.

This analysis follows the analysis of Pedersen [28]. The analysis allows for the application of any stress-crack opening relation using numerical integration to obtain the solution. The analysis takes into account combined axial force and moment on the cross section.

Consider a non-linear hinge with rectangular cross-section and depth h. The cross section is subjected to an external bending moment M per width and the axial force N per width of the element. As long as the tensile strength is not reached the element is assumed to behave linear elastically according to classic Bernouilli beam theory.

When the tensile strength is reached, it is assumed that a single crack is formed with a maximum tensile stress f_t at the crack tip. Figure 18 shows

FIGURE 18. The analysis according to the simplified approach by Pedersen. The non-linear hinge subjected to axial force and moment is shown along with the assumed stress distribution and the resulting forces in the different regions.

the assumed distribution of stresses where the post-peak tensile stress is a function of the crack width given by the stress-crack opening relationship, $\sigma_w(w)$. Note that it is assumed that the compressive zone remains in the linear elastic range.

As indicated in Fig. 18 it is assumed that the crack has a linear profile (see also Maalej and Li [33]), thus the crack opening angle φ^* is related to the crack mouth opening w_{cmod} and the length of the fictitious crack a as follows:

$$\varphi^* = \frac{w_{cmod}}{a}. \tag{5.3}$$

Now, the distribution of normal stresses within the cracked zone is given by the stress-crack opening relationship, $\sigma_w(w)$ and the resulting force per width of the cracked zone and the bending moment per width of the cracked zone taken at the crack tip, N_f and M_f respectively, can be obtained by integrating:

$$N_f = \frac{1}{\varphi^*} \int_0^{w_{cmod}} \sigma_w(u)\, du, \tag{5.4}$$

$$M_f = \frac{1}{(\varphi^*)^2} \int_0^{w_{cmod}} \sigma_w(u)u\, du. \tag{5.5}$$

It is now required that the crack opening angle corresponds to the total angular deformation of the non-linear hinge. With the given assumptions the depth of the tensile zone, $h - x_0$, (see Fig. 18) in the non-linear hinge may now be related to the crack mouth opening by:

$$h - x_0 = \frac{1}{\varphi}(\frac{f_t}{E}s + w_{cmod}) \tag{5.6}$$

where s is the length of the non-linear hinge.

The resulting force per width of the elastic compression zone is denoted N_c and the resulting force per width of the elastic tensile zone is denoted N_t:

$$N_c = \frac{\varphi E x_0^2}{2s}, \tag{5.7}$$

$$N_t = \frac{(f_t)^2 s}{2\varphi E}. \tag{5.8}$$

Equation (5.7) describes how N_c is related to φ and x_0: $N_c(\varphi, x_0)$. Equation (5.8) describes how N_t is related to φ: $N_t(\varphi)$. Equation (5.4) describes how N_f is related to φ and w_{cmod}: $N_f(\varphi, w_{cmod})$.

Denoting the resulting axial force per width of the element N, for a given angular deformation φ, the equilibrium of the section is written in the following way in order to determine the position of the neutral axis:

$$N_t(\varphi) + N_f(\varphi, w_{cmod}) - N_c(\varphi, x_0) = N. \tag{5.9}$$

The crack mouth opening w_{cmod} can be substituted from Eq. (5.6):

$$N_t(\varphi) + N_f(\varphi, x_0) - N_c(\varphi, x_0) = N. \tag{5.10}$$

Given φ and N the position of the neutral axis can be determined from Eq. (5.10).

Now the moment M relative to the center line of the cross section can be determined. The moment is given by:

$$M = (\frac{h}{2} - \frac{x_0}{3})N_c + (\frac{h}{6} + \frac{x_0}{3} - \frac{2a}{3})N_t + (\frac{h}{2} - a)N_f + M_f \tag{5.11}$$

where a is determined by Eqs. (5.3) and (5.6). Thus the result of the calculation is corresponding values of angular deformation, axial force, and bending moment:

$$M = M(\varphi, N), \tag{5.12}$$

and the solution constitutes the characteristics of the non-linear hinge.

Furthermore, results are obtained for fictitious crack length a, crack mouth opening w_{cmod} and stresses.

The non-linear Eq. (5.10) can be solved for x_0 using a simple numerical iteration technique, e.g. bisection. Furthermore, the involved integrations in Eqs. (5.4) and (5.5) can be carried out using a numerical integration scheme allowing for the use of any stress-crack opening relationship $\sigma_w(w)$.

5.3.2. Simplified approach by Casanova.

Casanova and Rossi [30] proposed a model which adopts the assumptions shown in Fig. 17(a) with respect to the angle at the faces of the non-linear hinge and the crack opening angle. In the model it is assumed that the angle formed by the crack varies according to the crack mouth opening and the depth of the crack:

$$\varphi = \frac{w_{cmod}}{a}. \tag{5.13}$$

The length s of the non-linear hinge in Casanova's model varies with the depth of the crack such that:

$$s = 2a. \tag{5.14}$$

The final assumption is related to the internal kinematics of the hinge. Two curvatures are considered, the elastic curvature of the un-cracked part of the hinge, κ_1, and the curvature in the cracked zone, κ_2. The elastic curvature is given by:

$$\kappa_1 = \frac{12M}{Eh^3} \tag{5.15}$$

where M is the moment per unit width in the beam.

The curvature in the cracked zone is given by:

$$\kappa_2 = \frac{\varepsilon_c}{x_0} \tag{5.16}$$

where ε_c is the strain at the extreme fibre in compression, and x_0 is the depth of the neutral axis at the crack.

The depth of the neutral axis in the un-cracked (elastic) zone in Casanova's model is based on linear elasticity. Thus, although $\varphi = \varphi^*$, the neutral axis, and therefore the curvature, are different at the faces of the non-linear hinge and at the crack.

The curvature in the un-cracked and the cracked part of the hinge is linked to the average curvature κ_m (see Eq. (5.1)) of the hinge by assuming a parabolic variation of the curvature along the non-linear hinge:

$$\kappa_m = \frac{2\kappa_1 + \kappa_2}{3}. \tag{5.17}$$

Combining Eqs. (5.13) to (5.17) leads to the basic constitutive relationship of the model proposed by Casanova and Rossi [30]:

$$w_{cmod} = 2\kappa_m a^2 = 2\left(\frac{2\kappa_1 + \kappa_2}{3}\right)a^2. \tag{5.18}$$

Equations (5.4) to (5.5) and (5.7) to (5.11) presented for Pedersen's model are directly applicable with Casanova's model when φ/s is replaced with κ_m. Again, the equilibrium equation (5.10) has to be solved by numerical iteration.

In the above a linear stress-strain relationship for the concrete in compression or in tension outside the cracked zone is adopted. In the general case where a non linear stress strain relationship for concrete in compression is chosen, a numerical integration over depth of the cross section can be carried out. This approach has been used by Massicote et al. [34] to predict the response of fibre reinforced slab elements.

5.3.3. Explicit formulation by Olesen.

It is possible to obtain a closed form solution for the non-linear hinge when using a multi-linear or bi-linear stress crack-opening relationship in combination with the kinematic assumption that the boundaries of the non-linear hinge remain plane while the fictitious crack plane deformation is governed by the stress-crack opening relationship as well as the overall angular deformation of the non-linear hinge and the length of the fictitious crack.

In particular a solution for the moment-rotation relationship in the case of zero axial force and a bi-linear stress-crack opening relationship was presented in Stang and Olseen [27]. The complete solution for the bi-linear stress-crack opening relationship including a non-zero axial force can be found in [32]. The derivation follows [27] closely.

The non-linear hinge is modelled as incremental layers of springs that act without transferring shear between each other, see Fig. 19. The vertical boundaries of the hinge are assumed to remain straight during deformation and the total angular deformation of the non-linear hinge is again denoted φ. The associated longitudinal deformation of the springs is denoted $u(x)$ where x is a vertical co-ordinate, see Fig. 19. The average curvature of the non-linear hinge, κ_m, is given by Eq. (5.1), while the mean longitudinal strain, $\varepsilon^*(x)$, is given by

$$\varepsilon^*(x) = \kappa_m(x - x_0) = \frac{u(x)}{s} \tag{5.19}$$

where x_0 is the co-ordinate of the neutral axis in the hinge. It is assumed that the hinge layers behave linear elastically as long as the tensile strength
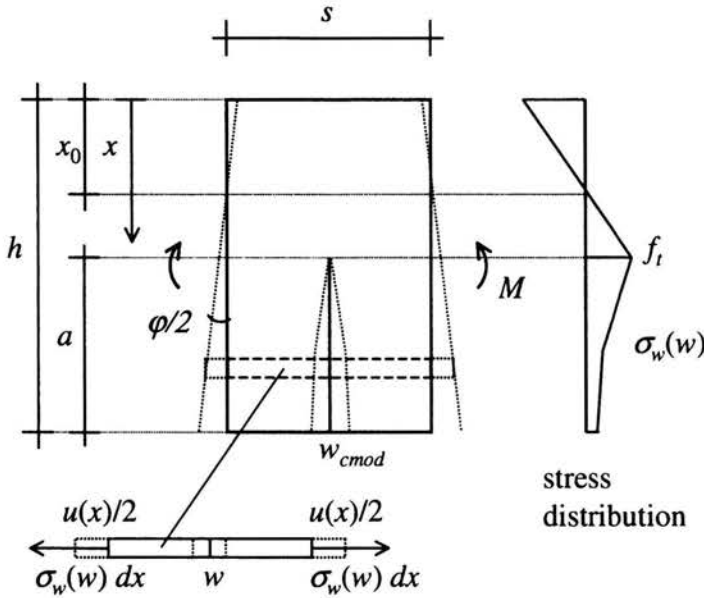
FIGURE 19. The modelling of the propagation of the fictitious crack through the non-linear hinge used in the explicit formulation. Below the non-linear hinge: illustration of an incremental horizontal layer of the band. To the right: the associated stress distribution.

f_t is not reached. When the stress reaches f_t a fictitious crack is assumed to form with a stress-crack opening relationship σ_w which is a function of the crack opening w which in turn is a function of x. The deformation u of a layer may then be obtained from

$$u(x) = \frac{\sigma_w(w(x))}{E}s + w(x). \tag{5.20}$$

Considering that the axial force is zero and that the stress-crack opening relation $\sigma_w(w)$ is the bi-linear function, Eq. (4.2), four different stress distributions develop in the cross section as the fictitious crack grows. The different phases are shown in Fig. 20. The phases are governed by the parameters x_1 and x_2 given by the general expression:

$$x_i = x_0 + \frac{1}{\varphi}[\varsigma_i - w_i(\psi_i - 1)], \qquad i = 1, 2, \tag{5.21}$$

where

$$\varsigma_i = \frac{\sigma_i s}{E}, \qquad \psi_i = \frac{\alpha_i s}{E}, \qquad i = 1, 2. \tag{5.22}$$
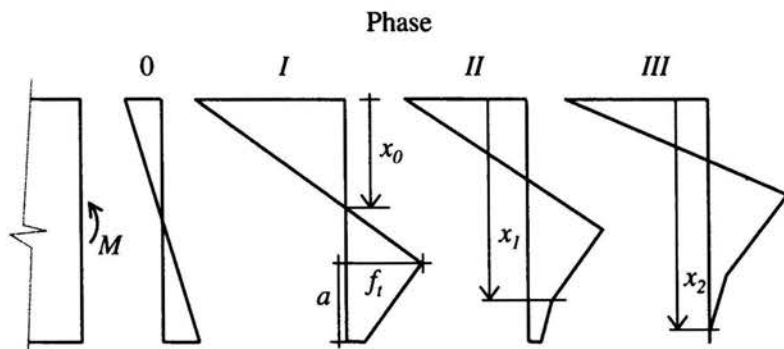
FIGURE 20. Definition of the four different phases of stress distribution experienced during crack propagation.

The following normalizations are introduced:

$$\mu = \frac{6}{f_t h^2 t} M, \qquad \theta = \frac{hE}{2sf_t}\varphi, \qquad \alpha = \frac{a}{h}, \qquad (5.23)$$

where a is the depth of the fictitious crack. The moment is normalized with the moment which causes the crack initiation while the angular deformation is normalized with the angular deformation at crack initiation. Given these normalizations the pre-crack elastic behaviour of the hinge is described by the relation $\mu = \theta$ with $0 \le \theta \le 1$. The complete solution in the three crack development phases is given below. For convenience the following properties b and c are introduced:

$$b = \frac{\sigma_2}{f_t}, \qquad (5.24)$$

$$c = (1 - b)(1 - \psi_1)/(\psi_2 - \psi_1). \qquad (5.25)$$

The analysis of the non-linear hinge is carried out with θ as the controlling parameter. Thus, the values of θ corresponding to phase transitions need to be known. Three different values are relevant, θ_{0-I}, θ_{I-II} and θ_{II-III}:

$$\theta_{0-I} = 1, \qquad (5.26)$$

$$\theta_{I-II} = \frac{1}{2}\left(1 - c + \sqrt{(1-c)^2 + \frac{c^2}{\psi_1 - 1}}\right), \qquad (5.27)$$

$$\theta_{II-III} = \frac{1}{2}\left(\frac{b}{\psi_2} + \sqrt{\frac{(1-b)^2}{\psi_1 - \psi_2} + \frac{b^2}{\psi_2}}\right). \qquad (5.28)$$

For phase I with $\theta_{0-I} \leq \theta \leq \theta_{I-II}$ the solution reads:

$$\alpha = 1 - \psi_1 - \sqrt{(1 - \psi_1)\left(\frac{1}{\theta} - \psi_1\right)}, \qquad (5.29)$$

together with:

$$\mu = 4\left(1 - 3\alpha + 3\alpha^2 - \frac{\alpha^3}{1 - \psi_1}\right)\theta - 3 + 6\alpha. \qquad (5.30)$$

For phase II with $\theta_{I-II} \leq \theta \leq \theta_{II-III}$ the solution reads:

$$\alpha = 1 - \psi_2 - \frac{1 - b}{2\theta} - \sqrt{(1 - \psi_2)\left(\frac{(1 - b)^2}{4\theta^2(\psi_1 - \psi_2)} - \psi_2 + \frac{b}{\theta}\right)}, \qquad (5.31)$$

together with:

$$\mu = 4\left(1 - 3\alpha + 3\alpha^2 - \frac{\alpha^3}{1 - \psi_2}\right)\theta - 3 + 6\alpha - \frac{(1 - b)\left(3\alpha^2 - \left(\frac{c}{2\theta}\right)^2\right)}{1 - \psi_2}. \qquad (5.32)$$

For phase III with $\theta_{II-III} \leq \theta$ the solution reads:

$$\alpha = 1 - \frac{1}{2\theta}\left(1 + \sqrt{\frac{(1 - b)^2}{\psi_1 - \psi_2} + \frac{b^2}{\psi_2}}\right), \qquad (5.33)$$

together with:

$$\mu = 4\left(1 - 3\alpha + 3\alpha^2 - \alpha^3\right)\theta - 3 + 6\alpha - 3\alpha^2$$
$$+ \frac{1}{4\theta^2}\left(1 - \frac{b}{\psi_2}\right)\left(1 - \frac{b}{\psi_2} + c\right)\left(1 + \frac{\psi_1 c}{1 - \psi_1}\right) + \left(\frac{c}{2\theta}\right)^2. \qquad (5.34)$$

A closed form solution for w_{cmod} – the crack opening at the mouth of the crack – is obtained in [32]. In a compact form this can be written as:

$$w_{cmod} = \frac{sf_t(1 - b_i + 2\alpha\theta)}{E(1 - \psi_i)} \qquad (5.35)$$

where $(b_i, \psi_i) = (1, \psi_1)$ in phase I, (b, ψ_2) in phase II and $(0, 0)$ in phase III.

With the simple drop-constant stress-crack opening relationship defined in Eq. (4.3) involving the residual strength σ_y the $\mu(\theta)$ relationship reduces to the simple relationship, all in phase I, i.e. for $\theta > 1$:

$$\mu(\theta) = \gamma\left(3 - 2\sqrt{\frac{\gamma}{\theta}}\right), \qquad (5.36)$$

with:

$$\gamma = \frac{\sigma_y}{f_t}. \tag{5.37}$$

Furthermore, in this case the solution for w_{cmod} can be written as

$$w_{cmod}(\theta) = (1 - \gamma + 2\alpha\theta)\frac{sf_t}{E}, \tag{5.38}$$

with the normalized crack length given by:

$$\alpha = 1 - \frac{1 - \gamma}{2\theta} - \sqrt{\frac{\gamma}{\theta}}. \tag{5.39}$$

5.3.4. Application of the non-linear hinge in structural analysis.
Structural calculations of e.g. beams [29, 30, 28, 31, 27, 23, 32], beams on elastic foundation [32] and pipes [28], can be done by introducing a non-linear hinge in the structure, prescribing the angular deformation on the non-linear hinge, using the non-linear hinge solution to solve for the generalized stresses at the non-linear hinge, establishing the linear elastic solution for the structure given the generalized stresses at the non-linear hinge and finally solving for the applied load and the total deformations. As an example, see Sec. 6 and the Annex in case of a simply supported beam subjected to 3 point loading.

The length of the non-linear hinge s has to be considered a fitting parameter for the calculations. In general the optimal length will depend on the type of structural element. The hinge width s in a beam has previously been assessed (cf. [31, 28]) using non-linear hinge models for plain as well as fibre reinforced concrete and it has been shown that $s = h/2$ is an adequate choice. Comparisons between the explicit model by Olesen, the simplified approach by [28] and the approach by [29] for the bi-linear stress-crack opening relationship show very similar results. Furthermore, all models compare favorably with a non-linear FEM analysis using the same bi-linear stress-crack opening relationship, see the Annex. This seems to indicate that, for a large number of stress-crack opening relationships, the simplified assumptions that the fictitious crack faces remain plane and that the deformation of the non-linear hinge is primarily due to the crack opening are reasonable.

5.4. Cross section with conventional reinforcement

The models presented in Sec. 5.3 were aimed at predicting the behaviour of cross sections reinforced only with fibres. In applications where conventional reinforcement is used with fibre concrete, additional assumptions related to the length of the non-linear hinge, the stress in the reinforcement at the crack, and the average curvature must be adopted.

In presence of reinforcement, FRC members exhibit multiple cracking until reinforcement yielding. At that point, one crack generally governs the member behaviour due to the softening nature of fibre concrete. The assumptions must enable modelling the member response at small and moderate crack opening. At small crack opening under service loads, both the maximum crack width and the stress level limits in the reinforcement can have a significant importance (e.g. for durability purposes or for the fatigue of the reinforcement, Bélanger [35]). In general, the ultimate load of a conventionally reinforced FRC member corresponds to the situation when the conventional reinforcement yields. At this stage the fibre contribution to the load carrying capacity can be significant. In both cases it is therefore essential for the assumptions adopted to be realistic and representative of the actual behaviour.

5.4.1. Crack spacing. In direct tension and in flexure, the observed crack spacing in the presence of fibres is less than in identical members without fibres [36, 37, 38]. Although formulations have been proposed to determine crack spacing in the presence of fibres, Moffat [37], further research has to be carried out in this area before a general formulation is available. However, attention should be drawn to the recent formulation of a so-called adaptive hinge model, Olesen [39], which essentially is a non-linear hinge (Sec. 5.3) that takes into account both the propagation of the fictitious crack and the debonding between re-bars and FRC. The reason for calling the model the adaptive hinge is that the width of the hinge adapts itself to the debonded region on both sides of the bending crack. The model also provides information about crack opening and average curvature of the adaptive hinge. However, the model has not yet been experimentally verified. Therefore, until such information is available, crack spacing has to be evaluated based on reasonable assumptions. The formulation proposed in Eurocode 2, [40], for the average crack spacing and described in Test and Design Methods for Steel Fibre Reinforced Concrete. Recommendations for the $\sigma - \varepsilon$ design method [8] gives an upper limit. Experimental evidence indicates that crack spacing in FRC members smaller than the member depth is observed, both in flexure and in direct tension. It is therefore proposed to adopt the following assumptions for crack spacing, s_{rm}:

$$s_{rm} = 50 + 0.25 k_1 k_2 \frac{\phi}{\rho_r} \qquad (5.40)$$

where ϕ is the bar diameter in mm whereas ρ_r, the effective reinforcement ratio, and parameters k_1 and k_2 are defined in [40].

The relationships presented in Sec. 5.3 for unreinforced concrete are applicable to members reinforced with conventional reinforcement. In this case the length of the non-linear hinge defined in Sec. 5.3 still applies to determine the response of the section. However in computing the deflection, Massicotte et al. [34] showed that more than one crack may govern the member behaviour and that a length equal to the member depth but not less than s or not less than the value given by Eq. (5.40) should be used. They also showed that adopting the variable non-linear hinge length presented by Casanova and Rossi [30] leads to reasonable results as compared to experimental results.

5.4.2. Reinforcement strains in the cracked region. Adopting Eurocode representation of the interaction between concrete and reinforcement allows us to consider reinforced FRC member behaviour as a weighted average between the cracked and uncracked regions. Therefore the strain in conventional reinforcement in the cracked zone is given by:

$$\varepsilon_{s2} = (d - x_0)\kappa_2 \qquad (5.41)$$

where d is the position of the reinforcement with respect to the compression face. This assumption is applicable with the simplified methods presented in Sec. 5.3.

5.4.3. Average curvature. The average curvature can be determined according to the recommendation [40], averaging the curvature at the crack and between cracks:

$$\kappa_m = (1 - \zeta)\kappa_1 + \zeta\kappa_2, \qquad (5.42)$$

with

$$\zeta = 1 - \beta_1\beta_2 \left(\frac{\sigma_{sr}}{\sigma_{s2}}\right)^2 \qquad (5.43)$$

where β_1 and β_2 are factors defined in [40], σ_{sr} is the stress in the reinforcement at the crack just after cracking whereas σ_{s2} is the current reinforcement stress at the crack. Curvatures κ_1 and κ_2 are computed in the uncracked and cracked regions respectively, using an iterative procedure, Massicotte et al. [34].

Alternatively, Eq. (5.17) proposed by [30] for FRC members only, can also be adopted to represent the average curvature over the non-linear hinge for members containing conventional reinforcement. This approach was used by Massicotte et al. [41] and showed good agreement with experimental results.

5.5. Limit states

5.5.1. Serviceability limit state. The serviceability limit state defines a maximum crack opening depending on the exposure class of the construction. Limiting crack openings are suggested in [8]. Both the case of steel fibre reinforced concrete with and without conventional reinforcement are covered. Code values may be adopted. Crack openings follow directly for the cross sectional analysis described above.

5.5.2. Ultimate limit state. In case of cross sections without conventional reinforcement the ultimate limit state in bending is determined simply by the ultimate load carrying capacity calculated according to the above-mentioned methods.

In the case of under-reinforced cross section, the ultimate load carrying capacity is usually reached at onset of reinforcement yielding. Beyond that point, the member exhibits a softening that is governed by the amount of reinforcement and the fibre concrete properties. At yielding of the reinforcement the concrete in compression can be first assumed to behave linear elastically which enables the use of the methods presented in Sec. 5.3. The maximum stress level in the concrete can then be checked. If the assumption is shown to be appropriate, the ultimate strength of the cross section determined with the methods presented above is adequate. In cases where the assumption of a linear behaviour in compression is not valid, the non-linearity of the concrete in compression should be taken into account as specified by codes for normal reinforced concrete members.

6. Beam analysis: load-deflection behavior

6.1. Analysis

In this Section the non-linear hinge is introduced in a simple beam without conventional reinforcement, loaded in three point bending and experiencing failure in bending, see Fig. 21.

Consider a beam with rectangular cross section with depth h, width t and span L. The deflection u is calculated as a sum of two terms:

$$u = u_e + u_c, \tag{6.1}$$

the elastic u_e and the cracking u_c related part of the deflection. This superposition of deformations is illustrated in Fig. 22.
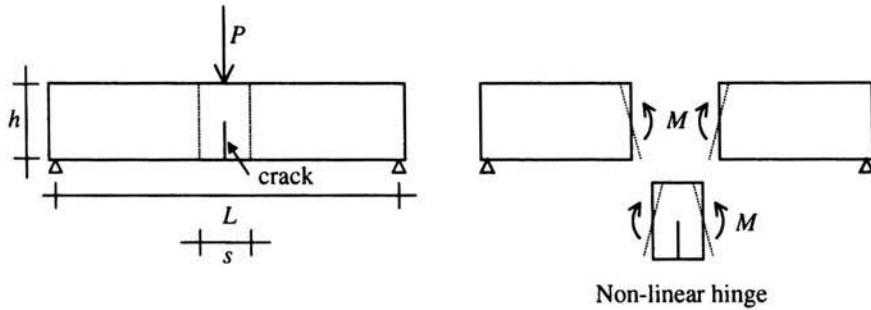
FIGURE 21. The principle of the non-linear hinge analysis in the case of a beam with rectangular cross section, no conventional reinforcement, subjected to three point bending. The beam geometry and loading is shown on the left hand side. On the right hand side it is shown how the beam is divided into a middle section of width s containing the non-linear hinge and the rest of the beam which is assumed to behave elastically.
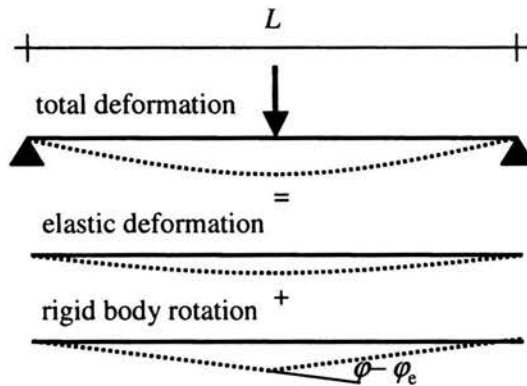

FIGURE 22. The principle of the superposition of elastic and cracking related deformation. The elastic deformation is calculated according to classical beam theory while the cracking related deformation is calculated from the deformation of the non-linear hinge, assuming that the rest of the beam rotates as stiff bodies.

According to classical beam theory u_e is related to the load P and the beam span L as follows:

$$u_e = \frac{PL^3}{48EI} \tag{6.2}$$

where E is Young's modulus of the FRC-material and I is the moment of inertia of the cross section. The cracking related part of the deflection u_c is calculated modelling the crack as a generalized plastic hinge as shown above.

In the calculation of this part the two halves of the beam are both assumed
to be rigid and rotate an angle ϕ:

$$\phi = \frac{\varphi - \varphi_e}{2} \tag{6.3}$$

where φ_e is the angular deformation of the non-linear hinge at the onset of
cracking given by:

$$\varphi_e = \frac{12sM}{Eth^3}, \tag{6.4}$$

while φ is the total angular deformation of the non-linear hinge prescribed
in the cross-sectional analysis. The deflection due to the rigid-body rotation
ϕ may be written in the form:

$$u_c = \phi \frac{L}{2}. \tag{6.5}$$

In the elastic case the deflection is given by $u = u_e$. When a crack has
developed the deflection is given by $u = u_e + u_c$. P is related to L and M by:

$$P = 4\frac{M(\varphi)}{L}. \tag{6.6}$$

In this case the elastic deflection can be obtained from Eqs. (6.2) and (6.6).

The entire load deflection diagram for a beam in three point bending can
be determined by prescribing angular deformations $\varphi > \varphi_{crack}$ of the non-
linear hinge, calculating the load on the beam from Eq. (6.6) and the two
parts of the deformation from Eqs. (6.2) and (6.5). It follows that the load
which initiates cracking P_{crack} is given by:

$$P_{crack} = f_t \frac{2h^2 t}{3L}. \tag{6.7}$$

In Eq. (6.6) any of the moment-rotation relationships described above
can be applied. Furthermore, it was shown in Stang and Olesen [23] how the
above analysis can be extended to cover the case of a beam with a notch.

Alternative approaches based on integration of the curvature along the
length of the beam can be adopted, Massicotte et al. [34].

7. Shear capacity: ultimate limit state

The shear capacity of FRC beams with conventional longitudinal reinforc-
ing bars has been analyzed extensively in the literature [30] by considering
the failure to occur due to crack propagation along known planes. Only such

cases will be considered in this Section since there is no generally accepted method for the determination of the shear capacity of FRC elements without conventional reinforcement. The approach of [30] to calculate the contribution from the fibres is described in the following.

Following Eurocode 2, [40], the ultimate shear load carrying capacity V_{Rd3} is taken to be the sum of the contributions of the member without shear reinforcement $V_{c,d}$, of the stirrups and/or inclined bars, $V_{w,d}$, and the steel fibres $V_{f,d}$:

$$V_{Rd3} = V_{c,d} + V_{w,d} + V_{f,d}. \tag{7.1}$$

The contributions of the member without shear reinforcement and the stirrups and/or inclined bars can be calculated according to Eurocode 2. See also [8].
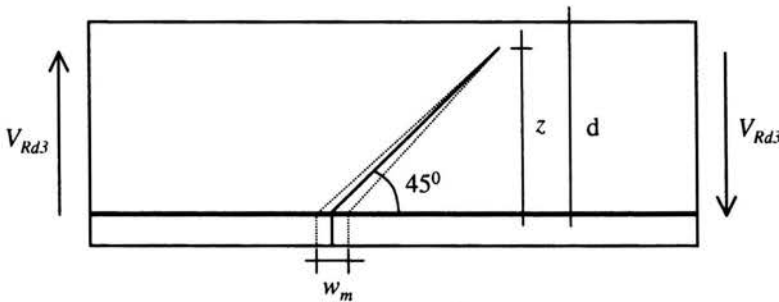

FIGURE 23. Assumed crack geometry in a beam with conventional, longitudinal reinforcement loaded to the ultimate shear loading capacity, V_{Rd3}. The crack is assumed to extend under 45^0, and the crack opening at the re-bar is limited to w_m.

Considering a rectangular cross section with width b, effective depth d (distance from the top of the beam to the reinforcing bars) and inner lever arm $z = 0.9d$, see Fig. 23, the fibre contribution $V_{f,d}$ is calculated from the design stress-crack opening relationship $\sigma_{w,d}(w)$ in the following way:

$$V_{f,d} = bz\overline{\sigma}_{p,d}(w_m), \tag{7.2}$$

with:

$$\overline{\sigma}_{p,d}(w_m) = \frac{1}{w_m} \int_0^{w_m} \sigma_{w,d}(u)\, du. \tag{7.3}$$

The quantity $\overline{\sigma}_{p,d}(w_m)$ is called the mean design residual stress at the crack width w_m and represents the mean value of the post-cracking stress between zero and w_m.

A definition of w_m is necessary to quantify the ultimate load-carrying capacity of the beam failing in shear. Experimental studies carried out with different geometries of steel FRC beams, reinforced with conventional longitudinal re-bars, have analyzed the onset of inclined cracks and the formation of concrete struts in compression, Casanova and Rossi [29]. According to the results, the spacing of these cracks is roughly equal to the inner lever arm of the beam and the ultimate crack opening is proportional to the height of the beam. Since the crack opening is controlled by the longitudinal reinforcement, it is proposed that the maximum crack opening be taken as:

$$w_m = \varepsilon_s z \tag{7.4}$$

where ε_s is the strain of the longitudinal reinforcement.

Since $V_{f,d}$ typically decreases with an increase in the maximum crack opening, the fibre contribution should be determined for a maximum allowable crack width. If the maximum strain in the longitudinal steel re-bar is taken to be 1%, then w_m should be taken as $0.009d$.

In order to obtain an equivalence relationship between conventional transverse reinforcement and fibres, we equate the contribution of $V_{w,d}$ to $V_{f,d}$ given in Eq. (7.2) to obtain an equivalent mean design residual stress, $\overline{\sigma}_{p,d}^*(w_m)$:

$$\overline{\sigma}_{p,d}^*(w_m) = \frac{V_{w,d}}{bz}. \tag{7.5}$$

This implies that the equivalent mean residual stress of $\overline{\sigma}_{p,d}^*(w_m)$ would yield the same load-carrying capacity as stirrups and/or inclined bars giving rise to $V_{w,d}$.

Furthermore, the equivalence in Eq. (7.5) can be used to extend the definition of the minimum shear stirrup reinforcement given in the Eurocode 2 by:

$$\overline{\sigma}_{p,d}^* + \rho_t f_{y,d} \geq 0.02 f_{c,d} \tag{7.6}$$

where $f_{c,d}$ is the design compressive strength of the concrete, $f_{y,d}$ is the design yield strength of the stirrups and ρ_t is the area of stirrup reinforcement per unit length.

8. Crack widths in slabs on grade under restrained shrinkage and temperature movement

Slabs on grade under restrained shrinkage and temperature movement is an important field of application for FRC. The present section presents an analysis for the crack opening at crack formation in such structures. Simple design formulae based on the drop-constant stress-crack opening relationship

Eq. (4.3) are presented but other more complicated formulae can readily be applied. The present example follows closely, Olesen and Stang [42].

An infinitely long slab of thickness h and unit width, cast onto a sub-base of e.g. graded gravel, is considered. The in-plane slab deformations are assumed to be governed only by shear stresses acting on the interface between the slab and the sub-base. Since the slab is infinitely long it will be completely restricted against longitudinal deformations. Thus, shrinkage or thermal strains developing in the slab will give rise to constant normal stresses throughout the length of the slab, assuming that the shrinkage and the thermal strains are homogeneous over the thickness. The normal stresses are assumed to be constant over the cross-section of the slab. If the imposed strain – shrinkage or thermal contraction or a combination of both – attains such a value that the normal stress equals the tensile strength f_t of the slab material, then a crack is initiated. The objective of this example is to determine the crack opening as a function of the parameters in the drop-constant stress-crack opening relationship.
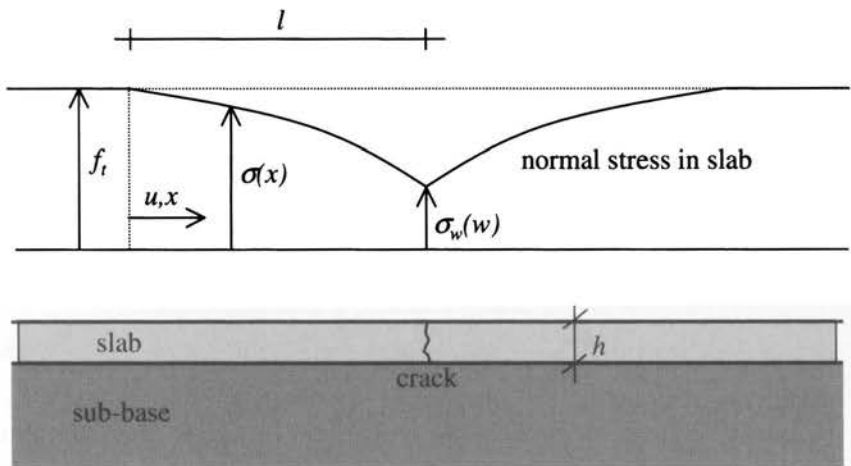

FIGURE 24. The stress distribution in an infinitely long, cracked slab restricted by shear stresses acting on the interface between slab and sub-base.

Figure 24 shows the slab together with the stress distribution in the slab after it has cracked. The shear reaction acting on the bottom face of the slab against the longitudinal deformation of the slab, $u(x)$, is modeled as a two-parameter linear function:

$$|\tau(x)| = \tau_0 + \xi|u(x)| \tag{8.1}$$

where τ_0 and ξ are constants describing cohesion and hardening on the slab-sub base interface, respectively. The shear reaction always acts in the opposite direction of $u(x)$. The normal stress σ is given by

$$\sigma = f_t + E\frac{du}{dx} \tag{8.2}$$

where E is the stiffness of the slab material. The differential equation governing the behaviour after crack initiation is readily established and reads as follows for the part of the slab to the left of the crack:

$$\frac{d^2u}{dx^2} = -\frac{|\tau|}{Eh}. \tag{8.3}$$

Since all deformations are negative, Eqs. (8.1) and (8.3) may be combined to furnish:

$$\frac{d^2u}{dx^2} - \frac{\xi}{Eh}u = -\frac{\tau_0}{Eh}, \quad u < 0. \tag{8.4}$$

With the boundary conditions $u(0) = 0$ and $\sigma(0) = f_t$ the solution to this equation may be written as:

$$u(x) = -\frac{\tau_0}{\xi}\left(\cosh(\lambda x) - 1\right), \quad \lambda^2 = \frac{\xi}{Eh}. \tag{8.5}$$

The state of stress in the slab is disturbed by the presence of the crack a distance l to either side of the crack. This length is unknown and depends on the opening of the crack, w, and a relation may be established by equating w to twice the displacement of the slab in $x = l$:

$$w = -2u(l) \Rightarrow \sinh(\lambda l) = \sqrt{\left(1 + \frac{w\xi}{2\tau_0}\right)^2 - 1}. \tag{8.6}$$

We may now calculate the stress in the slab at the crack as a function of the crack opening. Introducing Eq. (8.5) into (8.2) and evaluating at $x = l$ we arrive at:

$$\frac{\sigma(l)}{f_t} = 1 - \frac{E}{f_t}\sqrt{\frac{w}{2}\left(\frac{2\tau_0}{Eh} + \frac{\xi}{Eh}\frac{w}{2}\right)}. \tag{8.7}$$

This equation denotes the equilibrium path, and it states the necessary stress to act on the crack surface in order to ensure equilibrium of the slab at a certain crack opening w. The stress-crack opening relationship for the slab material is a function of w and is written as $\sigma_w(w)$. Thus, the crack opening which ensures equilibrium is established by the equation:
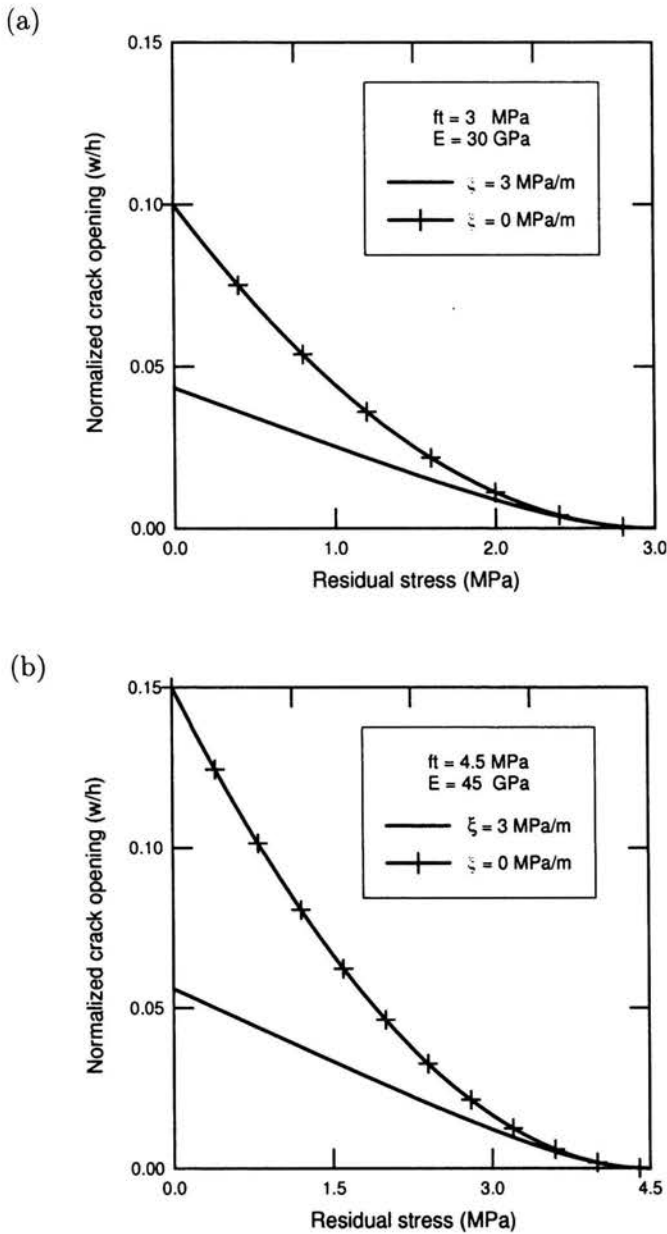
$$\sigma(l) = \sigma_w(w). \tag{8.8}$$

(a)

(b)

FIGURE 25. Crack opening divided by thickness of slab versus residual strength for two different strength levels, (a) $f_t = 3$ MPa, (b) $f_t = 4.5$ MPa. Applied parameter values: $h = 0.12$ m, $\tau_0 = 0.003$ MPa, $\xi = 0$ and 3 MPa/m.

This equation represents the general solution to the problem and is valid for any stress-crack opening relationship. Introducing the drop-constant stress-crack opening relationship Eq. (4.3), the following expressions for the equilibrium crack opening may be deduced:

$$
\frac{w}{h} = \begin{cases} 2\dfrac{\tau_0}{\xi h}\left(\sqrt{1 + \dfrac{\xi h}{E}\left(\dfrac{f_t - \sigma_y}{\tau_0}\right)^2} - 1\right) & \text{for } \xi \neq 0, \\[3ex] \dfrac{E}{\tau_0}\left(\dfrac{f_t - \sigma_y}{E}\right)^2 & \text{for } \xi = 0. \end{cases}
\tag{8.9}
$$

When using Eq. (8.9) it should be verified that the predicted crack opening w is less than w_{max} defined in the drop-constant stress-crack opening relationship applied (Eq. (4.3)).

Once the crack opening has been determined the corresponding crack spacing may be found via Eq. (8.6). The crack spacing will be in the interval $[l\,;\,2l]$. Note that the crack spacing increases with increasing w, thus, if we have large cracks they will be far apart, on the other hand, if we have narrow cracks they will be close together.

In Fig. 25 the normalized crack opening w/h is shown as a function of the residual strength σ_y. Two different slab materials are compared: one with a tensile strength of 3 MPa, the other with a 50% higher strength. The strength to stiffness ratio is assumed to be constant. It is observed that if the residual stress σ_y is the same in the two cases then the crack opening is larger when the tensile strength is higher. Note also that even for the same residual strength to tensile strength ratio, larger values of the crack opening are encountered when the tensile strength is increased.

A full scale test verifying the approach presented is described in [42] and experimental determination of the slab-sub base interface parameters τ_0 and ξ can be found in [43].

9. Conclusions and directions for future work

In the present document FRC materials (meaning tensions softening materials) have been investigated and the special problems related to material characterization, testing and structural analysis have been discussed.

Arguments have been presented pointing to a fracture mechanical based approach using the non-linear fracture mechanical model called the Fictitious Crack Model (FCM), using the so-called stress-crack opening relationship for characterization.

In the present document the stress-crack opening relationship, $\sigma_w(w)$, is applied for designing fibre reinforced concrete structural elements involv-

ing cross sections subject to combination of axial force, bending moment and shear force with or without conventional reinforcing bars. Furthermore shrinkage of slabs on grade is treated. The cross-sectional analysis with combined moment and axial force involves two main assumptions regarding:

1. The kinematic behaviour of the cracked cross section.
2. Representation of the stress-crack opening relationship.

With respect to the first assumption, numerical calculations reveal that the overall structural response is insensitive to the kinematic assumptions.

With respect to the second assumption, the results of the uniaxial tensile test should guide the choice of the representation of the stress-crack opening relationship.

Since fibre orientation can change from one structural application to another, care must be taken to ensure that the chosen relationship is representative of the material in the structural application under consideration. In general, the more representative the stress-crack opening relationship is, the more comprehensive the prediction of the structural behavior will be.

The design principles set forth in this document have been applied and verified in a number of studies, both experimental and numerical. Elements of experimental verification can be found in [28, 29, 30, 41, 42, 34, 37].

Further work is needed in the following areas:

1. Further analyze situations involving mixed mode crack propagation and opening (shear, torsion etc.).
2. Assess the sensitivity of the choice of analytical representation of stress-crack opening relationships.
3. Analyze the possibility of using the bending test as quality control in connection with the $\sigma_w(w)$ design method.
4. Assess time dependent effects such as fatigue, creep and durability.
5. Assess long term effects on the stress-crack opening relationship such as environmental impact and aging.

Annex

The basic continuum hypothesis underlying continuum mechanics of inhomogeneous materials (FRC materials in particular) is outlined in Fig. 26 together with an illustration of the relevant length scales, Fig. 27.
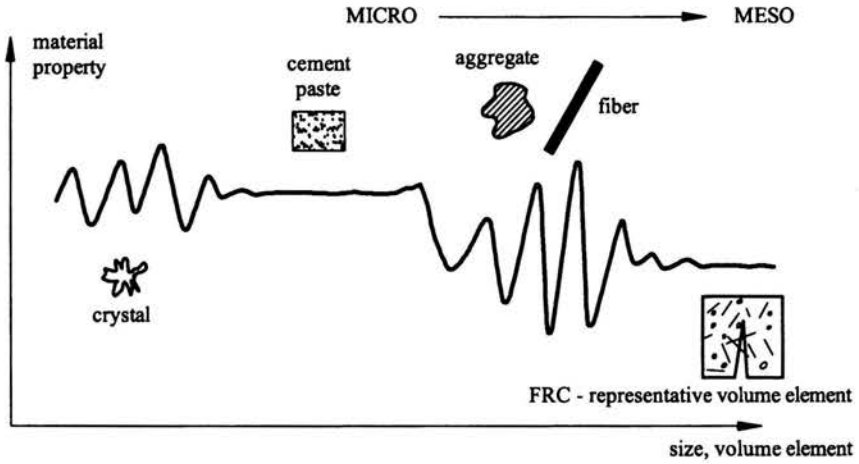
FIGURE 26. The concept of continuum, averaging and representative volume. The value of a material property will vary wildly when the volume element used for its determination is of the same order of magnitude as the constituent material structure. When the volume element is large enough to effectively average out the effect of the structure a representative volume element is obtained. Adapted from [44].
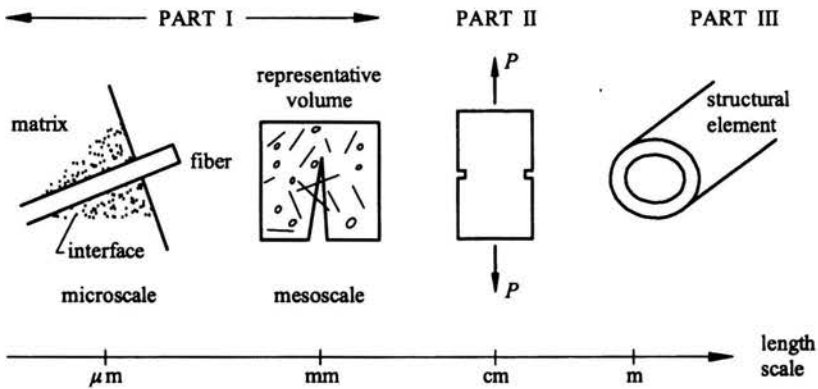

FIGURE 27. Illustration of various length scales in FRC material and structures, and approximate length scales which should be covered in an engineering approach to this material. Note that the presentative volume element is allowed to contain a crack indicating that part of the constitutive relations derived are set in the framework of fracture mechanics.

References

1. Test method for the measurement of the strain-softening behaviour of concrete under uniaxial compression, *Mater. Struc.*, Vol. 33, No. July, pp. 347–351, 2000, prepared by RILEM-TC 148-SCC, Strain Softening of Concrete - Test Methods for Compressive Softening, Chairman S.P. Shah.

2. M. GLAVIND and H. STANG, Evaluation of the complete compressive stress-strain curve for high strength concrete, in: *Fracture Processes in Concrete, Rock and Ceramics*, J. G. M. van Mier, J. G. Rots, and A. Bakker, Eds., London/New York: E & FN Spon, 1991, pp. 749–759.

3. A. E. NAAMAN, Fiber reinforcement for concrete, *Concrete International*, No. March, pp. 21–25, March 1985.

4. J. ROMUALDI and G. BATSON, Mechanics of crack arrest in concrete, *ASCE, J. Eng. Mech, Div.*, Vol. 89, pp. 147–168, 1963.

5. J. ROMUALDI and J. MANDEL, Tensile strength of concrete affected by uniformly distributed closely spaced short lengths of wire reinforcement, *J. American Concrete Institute*, Vol. 61, pp. 657–671, 1964.

6. V. LI, Post-crack scaling relations for fiber reinforced cementitious composites, *ASCE J. of Materials in Civil Engineering*, Vol. 4, No. 1, pp. 41–57, 1992.

7. Test and design methods for steel fiber reinforced concrete. recommendations for bending test, *Mater. Struc.*, Vol. 33, No. January-February, pp. 3–5, 2000, prepared by RILEM-Committee-TDF-162, Chairlady L. Vandewalle.

8. Test and design methods for steel fiber reinforced concrete. recommendations for σ-ε design method, *Mater. Struc.*, Vol. 33, No. March, pp. 75–81, 2000, prepared by RILEM-Committee-TDF-162, Chairlady L. Vandewalle.

9. H. STANG and J. OLESEN, *Test and Design Strategy for Fiber Reinforced Concrete Structure*, ser. Papers in Structural Engineering and Materials - A Centenary Celebration, Department of Structural Engineering and Materials, Technical University of Denmark, 2000, pp. 199–210.

10. Glassfibre reinforced concrete, practical design and structural analysis, Fachvereinigung Faserbeton e.V., Tech. Rep., 1995.

11. Recommended practice for glass fiber reinforced concrete panels, Prestressed Concrete Institute, Recommended Practice, 1987, prepared by PCI Committee on Glass Fiber Reinforced Concrete Panels, Chaiman Edwards S. Knowles.

12. B. KARIHALOO, *Fracture Mechanics & Structural Concrete*, ser. Concrete Design and Construction Series, Harlow, Essex, England: Longman Scientific & Technical, 1995.

13. A. HILLERBORG, M. MODÉER, and P. PETERSSON, Analysis of crack formation and crack growth in concrete by means of fracture mechanics and finite elements, *Cem. Concr. Res.*, Vol. 6, No. 6, pp. 773–782, 1976.

14. A. HILLERBORG, Analysis of fracture by means of the fictitious crack model, particularly for fibre reinforced concrete, *The Int. J. Cem. Comp.*, Vol. 2, No. 4, pp. 177–184, 1980.

15. V. LI, H. STANG, and H. KRENCHEL, Micromechanics of crack bridging in fiber reinforced concrete, *Mat. and Struc.*, Vol. 26, No. 162, pp. 486–494, 1993.

16. P. J. M. BARTOS and M. DURIS, Inclined tensile strength of steel fibres in a cement based composite, *Composites*, Vol. 25, pp. 945–951, November 1994.

17. J. KULLAA, Fibre-reinforced concrete under uniaxial tension, *Nordic Concrete Research*, Vol. 1/1994, No. 14, pp. 77–90, 1994.

18. D. LANGE-KORNBAK and B. L. KARIHALOO, Design of fiber-reinforced DSP mixes for minimum brittleness, *Adv. Cem. Bas. Mat.*, Vol. 7, pp. 89–101, 1998.

19. P. ROSSI and H. HARROUCHE, Mix design and mechanical behaviour of some steel-fiber-reinforced concretes used in reinforced concrete structures, *Materials and Structures*, Vol. 23, pp. 256–266, 1990.

20. P. ROSSI, Steel fiber reinforced concrete (SFRC): An example of French research, *ACI Mat. J.*, Vol. 91, No. 3, pp. 273–279, May-June 1994.

21. Test and design methods for steel fiber reinforced concrete. recommendations for uniaxial tension test. *Mater. Struc.*, Vol. 34, No. 235, pp. 3–6, January-February 2001, prepared by RILEM-Committee-TDF-162, Chairlady L. Vandewalle.

22. H. STANG and T. AARRE, Evaluation of crack width in FRC with conventional reinforcement, *Cement & Concrete Comp.*, Vol. 14, No. 2, pp. 143–154, 1992.

23. H. STANG and J. F. OLESEN, A fracture mechanics based design approach to FRC, in: *Fibre-Reinforced Concretes (FRC), BEFIB' 2000*, P. Rossi and G. Chanvillard, Eds., ENS - 61 Av. Pdt. Wilson, F-94235 Cachan Cedex, France: RILEM Publications S.A.R.L., 2000, pp. 315–324, proceedings of the Fifth International RILEM Symposium.

24. Test and design methods for steel fiber reinforced concrete. recommendations for bending test. *Mater. Struc.*, Vol. 33, No. 225, pp. 3–5, January-February 2000, prepared by RILEM-Committee-TDF-162, Chairlady L. Vandewalle.

25. P. NANAKORN, H. HORII, and S. MATSUOKA, A fracture mechanics-based design method for SFRC tunnel linings, *J. Materials, Conc. Struct., Pavements*, Vol. 30, No. 532, pp. 221–233, 1996.

26. Y. KITSUTAKA, Fracture parameters by polylinear tension-softening analysis, *J. Eng. Mechanics*, Vol. 123, No. 5, pp. 444–450, 1997.

27. H. STANG and J. F. OLESEN, On the interpretation of bending tests on FRC-materials, in: *Fracture Mechanics of Concrete Structures, Proceedings FRAMCOS-3*, H. Mihashi and K. Rokugo, Eds., Vol. 1, D-79104 Freiburg, Germany: Aedificatio Publishers, 1998, pp. 511–520.

28. C. PEDERSEN, New production processes, materials and calculation techniques for fiber reinforced concrete pipes, Ph.D. dissertation, Department of Structural Engineering and Materials, Technical University of Denmark, Series R, no. 14, 1996.

29. P. CASANOVA and P. ROSSI, Analysis of metallic fibre-reinforced concrete beams submitted to bending, *Materials and Structures*, Vol. 29, pp. 354–361, 1996.

30. P. CASANOVA and P. ROSSI, Analysis and design of steel fiber reinforced concrete beams, *ACI Structural. J.*, Vol. 94, No. 5, pp. 595–602, 1997.

31. J. P. ULFKJÆR, S. KRENK, and R. BRINCKER, Analytical model for fictitious crack propagation in concrete beams. *ASCE, J. Eng. Mech*, Vol. 121, No. 1, pp. 7–15, 1995.

32. J. F. OLESEN, Fictitious crack propagation in fiber-reinforced concrete beams, *Journal of Engineering Mechanics*, Vol. 127, No. 3, pp. 272–280, March 2001.

33. M. MAALEJ and V. C. LI, Flexural strength of fiber cementitious composites, *ASCE J. of Mat. in Civil Eng.*, Vol. 6, pp. 390–406, 1994.

34. B. Massicotte, K. Moffatt, and D. Bastien, Behaviour, analysis and design of fibre reinforced concrete structural members containing or not conventional reinforcement, Department of Civil, Geological and Mining Engineering, École Polytechnique de Montréal, Tech. Rep. Report EPM/GCS-2001-10, 2001, in press.

35. A. Bélanger, Conception de dalles de ponts avec armature réduite et béton de fibres d'acier, Master's thesis, École Polytechnique de Montréal, 2000.

36. N. Dzeletovic, Propriétés des dalles de ponts avec béton de fibres, Master's thesis, École Polytechnique de Montréal, 1998.

37. K. Moffatt, Calcul des dalles de pont avec béton de fibres d'acier, Master's thesis, École Polytechnique de Montréal, 2001.

38. L. Vandewalle, Cracking behaviour of concrete beams reinforced with a combination of ordinary reinforcement and steel fibers, *Mater. Struc.*, Vol. 33, pp. 164–170, April 2000.

39. J. F. Olesen, Cracks in reinforced FRC beams subject to bending and axial load, in: *Fracture Mechanics of Concrete Structures*, G. P.-C. J. G. v. M. René de Borst, Jacky Mazars, Ed., A.A. Balkema Publishers, 2001, pp. 1027–1033.

40. ENV-1992-1-1, Eurocode 2: design of concrete structures - part 1: General rules and rules for buildings, Tech. Rep., 1992, european pre standard.

41. B. Massicotte, A. Bélanger, and K. Moffatt, Analysis and design of SFRC bridge decks, in: *Fibre-Reinforced Concretes (FRC), BEFIB' 2000*, P. Rossi and G. Chanvillard, Eds., ENS - 61 Av. Pdt. Wilson, F-94235 Cachan Cedex, France: RILEM Publications S.A.R.L., 2000, pp. 263–272, proceedings of the Fifth International RILEM Symposium.

42. J. F. Olesen and H. Stang, Designing FRC slabs on grade for temperature and shrinkage induced cracks, in: *Fibre-Reinforced Concretes (FRC), BEFIB' 2000*, P. Rossi and G. Chanvillard, Eds., ENS - 61 Av. Pdt. Wilson, F-94235 Cachan Cedex, France: RILEM Publications S.A.R.L., 2000, pp. 337–346, proceedings of the Fifth International RILEM Symposium.

43. J. F. Olesen, FRC slabs on grade, full-scale tests, 1999, department of Structural Engineering and Materials, Technical University of Denmark, MUP2.

44. E. van der Giessen, Micromechanical modelling of composites, 1999, lecture notes, Course on Cement-based composites for the building industry.

———◇———